

Ultimate capabilities for compression of the waveform of a recoilless γ -ray photon into a pulse sequence in an optically deep vibrating resonant absorber

I. R. Khairulin,^{1,2} V. A. Antonov,^{2,3} Y. V. Radeonychev,^{2,1,4,*} and Olga Kocharovskaya⁵

¹*N. I. Lobachevsky State University of Nizhny Novgorod, 23 Gagarin Avenue, Nizhny Novgorod 603950, Russia*

²*Institute of Applied Physics of the Russian Academy of Sciences, 46 Ulyanov Street, Nizhny Novgorod 603950, Russia*

³*Prokhorov General Physics Institute of the Russian Academy of Sciences, 38 Vavilov Street, Moscow 119991, Russia*

⁴*Kazan E.K. Zavoisky Physical-Technical Institute of the Kazan Scientific Center of the Russian Academy of Sciences, 10/7 Sibirsky tract, Kazan 420029, Russia*

⁵*Department of Physics and Astronomy and Institute for Quantum Studies and Engineering, Texas A&M University, College Station, Texas 77843-4242, USA*



(Received 5 July 2018; published 31 October 2018)

Recently, an exponentially decaying waveform (the time dependence of detection probability) of a Mössbauer γ -ray photon was transformed into a regular sequence of short pulses in a sinusoidally vibrating recoilless resonant absorber [F. Vagizov, V. Antonov, Y. V. Radeonychev, R. N. Shakhmuratov, and O. Kocharovskaya, Coherent control of the waveforms of recoilless γ -photons, *Nature (London)* **508**, 80 (2014)]. In the present paper, we show that the peak amplitude of the pulses can be considerably increased via joint adjustment of optical depth of the absorber and the initial phase of its vibration. This is due to reduction of the photoelectric absorption and maximizing the constructive temporal interference of spectral content of the single-photon wave packet in an optically deep absorber. The ultimate capabilities for transforming a waveform of a 14.4-keV photon from a ^{57}Co radioactive source into a regular train of pulses in a harmonically vibrating ^{57}Fe recoilless resonant absorber are discussed. We show that the shortest pulse duration, produced by this technique, is limited by the highest available vibration frequency of a piezoelectric transducer and at present can be as short as 7.7 ps. The maximum achievable detection probability of the transformed photon at the experimentally feasible conditions is more than two times higher than peak detection probability of the photon emitted by the source and nearly 5.5 times higher than obtained in the above reference.

DOI: [10.1103/PhysRevA.98.043860](https://doi.org/10.1103/PhysRevA.98.043860)

I. INTRODUCTION

Hard-x-ray and γ -ray optics is an attractive and rapidly growing branch of physics, which gives rise to numerous applications in material science, chemistry, biology, medicine, and modern technologies. Extremely short wavelengths of hard-x-ray- γ -ray photons allow investigating material structure at atomic scales, while the narrow bandwidth of Mössbauer radiation (for example, a bandwidth of emission of a ^{57}Co radioactive source with photon energy 14.4 keV is about one MHz, which corresponds to 3×10^{-12} of its carrier frequency) permits precise measurements of local electric and magnetic fields, energy structure, and hyperfine interactions in solids and on their surfaces.

In recent years, a growing interest in these studies was motivated by penetration of concepts and ideas of coherent and quantum optics into the x-ray range of the electromagnetic spectrum. Earlier experimental achievements in this field include demonstrations of the Autler-Townes effect [1], γ -ray echo via abrupt shift of a nuclear absorber [2], controllable storage and release of nuclear excitation by switch of the magnetic field direction [3], electromagnetically induced transparency via a nuclear level anticrossing [4], slowing down of the γ -ray photon in a nuclear absorber with a split line [5],

and other effects discussed in the review [6]. Recent experimental advances include demonstration of parametric down-conversion in the Langevin regime [7], cavity electromagnetically induced transparency [8], collective Lamb shift [9], vacuum-assisted generation of atomic coherences [10], single-photon revival in nuclear absorbing sandwiches [11], phase-sensitive measurements characterizing the quantum state of a nuclei at hard-x-ray energies [12], group velocity control for 14.4-keV-energy photons [13], spectral enhancement of x-ray radiation via a moving absorber [14], and demonstration of a strong coupling between two nuclear polariton modes [15]. Also, a number of important effects were theoretically predicted recently including dynamical control of x-ray polarization qubits by nuclear Mössbauer resonance [16], heralded entanglement between two crystal-hosted macroscopic nuclear ensembles [17], as well as mapping and storing x-ray pulses in a thin-film planar x-ray cavity with an embedded resonant nuclear medium [18].

Recently, a possibility for coherent manipulation of the waveform (the time dependence of detection probability) of a Mössbauer γ -ray photon in a harmonically vibrating recoilless resonant absorber was shown both theoretically and experimentally [19]. In particular, (i) transformation of the exponentially decaying waveform of an incident 14.4-keV photon into a regular sequence of nanosecond pulses, and (ii) splitting of a single γ -ray photon into a double-spike pulse were shown. However, in the proof-of-principle experiment

*Corresponding author: radion@appl.sci-nnov.ru

[19] neither the absorber optical depth nor the initial phase of its vibration (the phase of vibration at the moment, when the front of the single-photon wave packet enters the medium) was optimized.

Further development of this approach was presented in [20], where an analytical solution was derived for the waveform of a γ -ray photon transmitted through the vibrating recoilless resonant absorber under the conditions realized in [19]. It was shown that bunches of a predetermined number of pulses can be produced, and the possibilities for using them in quantum information processing were discussed. The theoretical results were confirmed experimentally.

In [21,22], transformation of a continuous flow of γ -ray photons emitted by a high-activity source into a periodic pulse train was considered. In those papers, the possibilities to improve the peak intensity, duration, and shape of pulses with respect to the proof-of-principle experiment [19] were discussed. It was proposed (i) to increase an optical depth of the resonant absorber [22] and (ii) to use several sequentially placed resonant absorbers [21]. In particular, a possibility to increase the pulse peak intensity due to phase matching of the vibrational sidebands of γ radiation via the absorber dispersion was discussed [21,22].

Nevertheless, the optimal conditions for transformation of a single-photon waveform into a train of pulses taking into account propagation effects in an optically deep medium were not analyzed yet. At the same time, it is well known that in an optically deep absorber the exponentially decaying waveform of a photon transforms into a sequence of dips and humps, which is called “dynamical beats,” and originates from spectrally selective interaction of the photon field with the resonant nuclei [23]. With increasing absorber optical depth the dynamical beats shrink towards the front of the photon waveform (the dips and humps alternate faster). If the absorber vibrates under the conditions realized in [19], the produced pulses interfere with the dynamical beats. As a result, some of the pulses can be enhanced or suppressed. As shown in [19], the initial phase of the absorber’s vibration determines the position of the pulses in respect to the front of the waveform, and hence to the dynamical beats. Therefore, tuning both the initial phase of vibration and the optical depth of the absorber allows matching one or several pulses arisen due to vibration with humps of dynamical beats. As shown below, such a constructive interference can noticeably enlarge the pulse height.

In the present paper we study the possibilities to improve characteristics of pulses, which are produced from a single-photon waveform in a vibrating recoilless resonant absorber, via joint optimization of (i) the optical depth of the absorber responsible for the dynamical beats and (ii) the initial phase of vibration determining the position of the produced pulses with respect to dynamical beats. We also consider the possibility to use resonant dispersion of the absorber for increasing the pulse intensity in the single-photon regime.

The paper is organized as follows. In Sec. II we present the theoretical model. In Sec. III we derive an analytical solution for this model describing transformation of the exponentially decaying waveform of a Mössbauer photon into a regular sequence of short pulses taking into account propagation effects in an optically deep recoilless resonant absorber. On the basis of this solution we discuss physical mechanisms

which allow increasing the pulse height. In Sec. IV we find analytically and numerically the optimal parameter values for maximizing the peak detection probability of the photon for feasible experimental conditions, including conditions for producing the shortest pulses and conditions of the proof-of-principle experiment [19]. In Sec. V we discuss another physical mechanism leading to enhancement in the temporal detection probability. In Sec. VI we summarize the results.

II. THEORETICAL MODEL

Let us consider transformation of a 14.4-keV photon, emitted by a ^{57}Co Mössbauer radioactive source, in a recoilless ^{57}Fe resonant absorber, oscillating along the direction of propagation of Mössbauer radiation. The relevant energy levels of the source are shown in the left-hand side of Fig. 1(a). The ^{57}Co radioactive nuclide decays via electron capture producing a ^{57}Fe nucleus in the state $|c\rangle$ which decays with lifetime $T_c \simeq 12$ ns to the state $|b\rangle$, emitting a 122-keV γ -ray photon. Subsequently, the state $|b\rangle$ decays with lifetime $T_s \simeq 141$ ns to the ground state $|a\rangle$, emitting a 14.4-keV photon. Detection of a 122-keV photon determines the instant of formation of the state $|b\rangle$. It is chosen to be a time origin, $t_0 = 0$, for the time dependence of probability for detecting the 14.4-keV photon, $N_s(t)$, that is proportional to the coincidence count rate of the 14.4-keV photons emitted from the source:

$$N_s(t) = \frac{1}{T_s} \theta(t) \exp\{-t/T_s\}, \quad (1)$$

where $\theta(t)$ is the unit step function and T_s is the decay time of the state $|b\rangle$. After passing through a diaphragm, viewed in a small solid angle, the electric field of the photon can be represented in the form [23–27] [Fig. 1(b), upper part]

$$E_s(\tau_{\text{lab}}) = \frac{1}{2} E_0 \theta(\tau_{\text{lab}}) e^{-i(\omega_s + \Gamma_s/2)\tau_{\text{lab}} + i\varphi_0} + \text{c.c.}, \quad (2)$$

where E_0 is the field amplitude, $\tau_{\text{lab}} = t - z_{\text{lab}}/c$ is the local time in the laboratory reference frame, z_{lab} is the coordinate along the direction of the field propagation in the laboratory reference frame, $\Gamma_s = 1/T_s$ is the radiation bandwidth ($\Gamma_s/(2\pi) \simeq 1.13$ MHz for the ^{57}Fe nuclide), ω_s is the carrier frequency of the field corresponding to the wavelength $\lambda_s \simeq 0.86$ Å, and φ_0 is the random initial phase of the field. In Eq. (2) we neglected (i) the value z_s/c [where $z_s = z_0 + V_s t$ is the coordinate of the emitting nucleus that can be moved with constant velocity V_s , Fig. 1(b)] in the argument of the unit step function and (ii) the value $\Gamma_s z_s/(2c)$ in the exponent of the exponential function. Both approximations are valid at the propagation distances $z_s \ll 2c/\Gamma_s$ (in the case of ^{57}Fe , $2c/\Gamma_s \simeq 84.5$ m).

Let us consider propagation of the photon through the resonant absorber. The absorber constitutes a foil of stainless steel enriched by the resonant ^{57}Fe nuclei [Fig. 1(a) right side], fixed on a piezoelectric plate and uniformly (pistonlike) vibrating with frequency Ω along the direction of the photon propagation [Fig. 1(b)]. The thickness of the film, L , satisfies the inequality $L \ll 2\pi V_{\text{sound}}/\Omega$, where V_{sound} is the speed of sound in stainless steel. Consequently, the absorber vibrates as a whole according to

$$z_{\text{lab}} = z_a + R \sin(\Omega t + \vartheta_0), \quad (3)$$

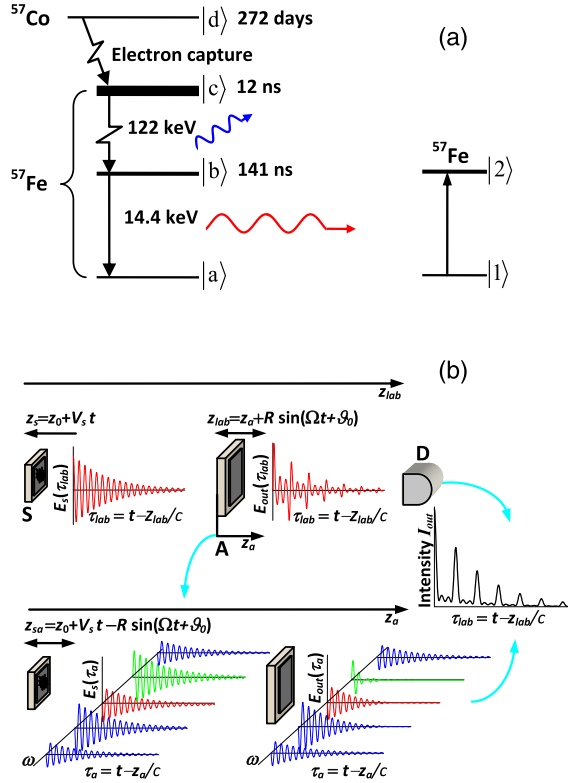


FIG. 1. (a) The energy diagram in the left side of this figure illustrates a decay of the ^{57}Co nucleus with a half-life of $T_{1/2} \simeq 272$ days from the state $|d\rangle$ to the state $|c\rangle$, followed by a cascade decay: $|c\rangle \rightarrow |b\rangle$ and $|b\rangle \rightarrow |a\rangle$ with emission of 122- and 14.4-keV photons (shown by blue and red lines, respectively). The energy diagram in the right side of this figure shows the quantum transition in the ^{57}Fe nucleus from the ground state $|1\rangle$ to the excited state $|2\rangle$ induced by a recoilless 14.4-keV photon. (b) Illustration of the experiment [19] for transformation of the exponentially decaying single-photon waveform into the regular pulse sequence in the laboratory reference frame (upper part) and in the reference frame of the vibrating absorber (lower part). Radioactive source “S” (a foil with ^{57}Co radionuclide) emits a 14.4-keV recoilless γ -ray photon (red pulse). A stainless steel foil “A” with ^{57}Fe nuclei vibrates in the laboratory reference frame along the propagation axis z_{lab} according to Eq. (3). The source is uniformly moved at velocity V_s to properly shift the carrier frequency of the photon with respect to the resonance frequency of the absorber due to the Doppler effect. At the exit from the absorber the quasimonochromatic single-photon wave packet turns into a regular pulse train. Its waveform is registered by detector “D.” This effect has clear interpretation in the reference frame comoving with the absorber (lower part). In the absorber reference frame a field of the emitted photon looks like a set of quasimonochromatic components described by Eq. (5c). All components are phase locked except for one antiphased component marked by a green color. Due to the uniform motion of the source, the antiphased (green) component is tuned to the resonance with an absorber’s transition. At the exit from the absorber it is strongly attenuated and transformed into the dynamical beats. Influence of the absorber resonance on the off-resonant components in the optically deep absorber also leads to their dynamical beats [see Eqs. (19)]. Temporal interference of the output spectral components results in a pulsed photon’s waveform that is the same in both reference frames (see the text).

where z_a is the coordinate in the vibrating reference frame, R is the amplitude, and ϑ_0 is the initial phase of the absorber’s vibration. The absorber’s motion is nonrelativistic, $R\Omega \ll c$ (where c is the speed of light in vacuum), therefore time in the vibrating reference frame is the same as in the laboratory reference frame. Substituting (3) into (2) allows one to write the electric field of the emitted photon in the vibrating reference frame as a frequency-modulated field:

$$E_s(\tau_a) = \frac{1}{2} E_0 \theta(\tau_a) e^{-\Gamma_s \tau_a / 2} e^{-i[\omega_s \tau_a - p \sin(\Omega \tau_a + \vartheta_0) - \varphi_0]} + \text{c.c.}, \quad (4)$$

where $\tau_a = t - z_a/c$ is the local time in the vibrating reference frame, and $p = 2\pi R/\lambda_s$ is the index of modulation of the resonant transition frequency. In Eq. (4) we neglected both the sinusoidal term in the step function and the amplitude modulation of the photon field, because of nonrelativistic motion of the absorber. According to (4), in the reference frame of the vibrating absorber the field of the incident photon acquires harmonic frequency modulation with a modulation frequency Ω . We assume that there is no reflection of the field from the absorber’s surface since the dielectric permittivity of the absorber’s material in the γ -ray range is very close to unity. Therefore in the vibrating reference frame at the entrance to the absorber, $z_a = 0$, the frequency-modulated photon field coincides with the emitted field (4) and can be represented in the form

$$E_{\text{inc}}(\tau_a) = \frac{1}{2} A_{\text{inc}}(\tau_a) e^{-i\omega_s \tau_a} + \text{c.c.}, \quad (5a)$$

$$A_{\text{inc}}(\tau_a) = E_0 e^{i\varphi_0} \theta(\tau_a) \exp\{-\Gamma_s \tau_a / 2\} \times \exp\{ip \sin(\Omega \tau_a + \vartheta_0)\}, \quad (5b)$$

where $A_{\text{inc}}(\tau_a)$ is the slowly varying complex amplitude of the incident field, $|dA_{\text{inc}}/d\tau_a| \ll \omega_s |A_{\text{inc}}|$. Using the Jacobi-Anger expansion, the incident field can be considered as a single-photon wave packet composed of a set of the exponentially decaying spectral components with equidistant carrier frequencies [Fig. 1(b), lower part]:

$$E_{\text{inc}}(\tau_a) = \frac{1}{2} \sum_{n=-\infty}^{\infty} \theta(\tau_a) E_0 J_n(p) e^{-\Gamma_s \tau_a / 2} \times e^{-i[(\omega_s - n\Omega)\tau_a - n\vartheta_0 - \varphi_0]} + \text{c.c.}, \quad (5c)$$

where $J_n(p)$ is the Bessel function of the first kind of order n . Applying Fourier transform to Eq. (5b), $A_{\text{inc}}(\omega) = \frac{1}{2\pi} \int_{-\infty}^{\infty} A_{\text{inc}}(\tau_a) e^{i\omega \tau_a} d\tau_a$, one gets the complex amplitude of a monochromatic frequency constituent of the single-photon wave packet:

$$A_{\text{inc}}(\omega) = \frac{E_0}{2\pi} \sum_{n=-\infty}^{\infty} \frac{J_{-n}(p) e^{i(\varphi_0 - n\vartheta_0)}}{-i(\omega - n\Omega) + \Gamma_s / 2}. \quad (5d)$$

As follows from (5d), in the reference frame of the vibrating absorber the quasimonochromatic incident field (2) can be considered as a comb of equidistant spectral components separated by the frequency of vibration. The n th component has the central frequency $\omega_n = \omega_s + n\Omega$, relative amplitude $|J_{-n}(p)|$, and Lorentz shape with bandwidth Γ_s . The phase at its central frequency, ω_n , at $\tau_a = 0$ will be referred to below as the central phase of the n th spectral component. For a fixed

value of modulation index, p , there are approximately $2p + 1$ spectral components with considerably nonzero amplitudes.

Interaction of the photon with a resonant nuclear transition from the ground state, $|1\rangle$, to the excited state, $|2\rangle$, of ^{57}Fe nuclei of the absorber [Fig. 1(a), right side] can be described by a master equation for the quantum coherence between these states, ρ_{21} [19,25–27]:

$$\frac{d\rho_{21}}{dt} + (i\omega_a + \gamma_a)\rho_{21} = in_{12} \frac{d_{21}E}{\hbar}, \quad (6)$$

where ω_a is the frequency of the resonant transition $|1\rangle \leftrightarrow |2\rangle$, which can differ from the central frequency of the source, ω_s , due to isomeric shift or Doppler shift produced by a motion of the absorber relative to the source with a constant velocity V_s [Fig. 1(b)]; γ_a is the half width of the spectral line of the resonant transition; $n_{12} = \rho_{11} - \rho_{22}$ is the population difference between the states $|1\rangle$ and $|2\rangle$; d_{21} is the dipole moment of the resonant transition; E is the electric field of the photon inside the medium; and \hbar is Planck's constant. Excitation of the quantum coherence, ρ_{21} , results in resonant macroscopic polarization of the medium:

$$P = f_a N d_{12} \rho_{21} + \text{c.c.}, \quad (7)$$

where f_a is the Lamb-Mössbauer factor (probability of Mössbauer effect) in the absorber's material, N is the concentration of the resonant nuclei, and $d_{12} = d_{21}^*$. In turn, the resonant polarization of the medium, P , leads to transformation of the photon field, E , in accordance with the wave equation

$$\frac{\partial^2 E}{\partial z_a^2} - \frac{1}{c'^2} \frac{\partial^2 E}{\partial t^2} = \frac{2\delta_e}{c'} \frac{\partial E}{\partial t} + \frac{4\pi}{\varepsilon c'^2} \frac{\partial^2 P}{\partial t^2}, \quad (8a)$$

where ε is the nonresonant dielectric permittivity of the absorber's material, $c' = c/\sqrt{\varepsilon}$ is the speed of light in the medium, and δ_e is the photoelectric absorption coefficient.

Let us change the independent variables from (z_a, t) to (z_a, τ'_a) , where $\tau'_a = t - z_a/c'$. In such a case, wave equation (8a) takes the form

$$\frac{\partial^2 E}{\partial z_a^2} - \frac{2}{c'} \frac{\partial^2 E}{\partial z_a \partial \tau'_a} = \frac{2\delta_e}{c'} \frac{\partial E}{\partial \tau'_a} + \frac{4\pi}{\varepsilon c'^2} \frac{\partial^2 P}{\partial \tau_a'^2}, \quad (8b)$$

while the equation for the quantum coherence (6) retains its form except for the replacement $t \rightarrow \tau'_a$. Let us further use approximation of the slowly varying complex amplitude:

$$\begin{aligned} E(z_a, \tau'_a) &= \frac{1}{2} \tilde{E}(z_a, \tau'_a) e^{-i\omega_s \tau'_a} + \text{c.c.}, \\ P(z_a, \tau'_a) &= \frac{1}{2} \tilde{P}(z_a, \tau'_a) e^{-i\omega_s \tau'_a} + \text{c.c.}, \\ \rho_{21}(z_a, \tau'_a) &= \tilde{\rho}_{21}(z_a, \tau'_a) e^{-i\omega_s \tau'_a}, \end{aligned} \quad (9)$$

where $|\partial \tilde{F}/\partial \tau'_a|$, $c'|\partial \tilde{F}/\partial z_a| \ll \omega_s |\tilde{F}|$, and \tilde{F} stands for \tilde{E} , \tilde{P} , and $\tilde{\rho}_{21}$. This approximation is well satisfied in the considered case, since $\omega_s \gg \Gamma_s, p\Omega$. Under this approximation the wave equation (8b) takes the form

$$\frac{\partial \tilde{E}}{\partial z_a} + \delta_e \tilde{E} = i \frac{2\pi\omega_s}{\varepsilon c'} \tilde{P}, \quad (10)$$

where we took into account that $\delta_e \ll \omega_s/c'$. Equation (6) takes the form

$$\frac{d\tilde{\rho}_{21}}{d\tau'_a} + (i[\omega_a - \omega_s] + \gamma_a)\tilde{\rho}_{21} = in_{12} \frac{d_{21}\tilde{E}}{2\hbar}, \quad (11)$$

which also implies the rotating-wave approximation, $|\omega_a - \omega_s| \ll \omega_s$, while the relation between the amplitudes of quantum coherence and macroscopic polarization (7) is given by

$$\tilde{P} = 2f_a N d_{12} \tilde{\rho}_{21}. \quad (12)$$

Let us seek for a solution of the system (10)–(12) in the form

$$\tilde{F}(z_a, \tau'_a) = \int_{-\infty}^{\infty} \tilde{F}(z_a, \omega) e^{-i\omega\tau'_a} d\omega, \quad (13a)$$

where \tilde{F} stands for \tilde{E} , \tilde{P} , and $\tilde{\rho}_{21}$, and

$$\tilde{F}(z_a, \omega) = \tilde{F}_0(\omega) \exp\{-[\delta_e + g(\omega)]z_a\}. \quad (13b)$$

Equations (10)–(13) give us

$$g(\omega) = \frac{2\pi f_a n_{12} N |d_{12}|^2 \omega_s}{\hbar c \sqrt{\varepsilon} [\gamma_a + i(\omega_a - \omega_s - \omega)]}. \quad (14)$$

In turn, the value of $\tilde{E}_0(\omega)$ is determined from the boundary condition at the front edge of the medium, $z_a = 0$, which is $\tilde{E}_0(\omega) = A_{\text{inc}}(\omega)$, where $A_{\text{inc}}(\omega)$ is determined by Eq. (5d). Consequently, we find the slowly varying amplitude of the single-photon wave packet inside the medium in the form

$$\begin{aligned} \tilde{E}(z_a, \tau'_a) &= \frac{E_0}{2\pi} e^{-\delta_e z_a} \sum_{n=-\infty}^{\infty} J_n(p) e^{i(\varphi_0 + n\vartheta_0)} \\ &\times \int_{-\infty}^{\infty} \frac{\exp\{-g(\omega)z_a - i\omega\tau'_a\}}{-i(\omega + n\Omega) + \Gamma_s/2} d\omega. \end{aligned} \quad (15)$$

Its intensity behind the absorber is $I_{\text{out}}(\tau_a) = \frac{c}{8\pi} |\tilde{E}(z_a = L, \tau_a)|^2$ where τ'_a in (15) is replaced with τ_a .

Let us return to the laboratory reference frame and look for the field of the photon behind the absorber in the form

$$E_{\text{out}}(\tau_{\text{lab}}) = \frac{1}{2} A_{\text{out}}(\tau_{\text{lab}}) e^{-i\omega_s \tau_{\text{lab}}} + \text{c.c.}, \quad (16)$$

where $\tau_{\text{lab}} = t - z_{\text{lab}}/c$, and A_{out} is the slowly varying amplitude of the output field. The substitution $\tau_{\text{lab}} \rightarrow \tau_a \rightarrow \tau'_a$, and use of the boundary condition in the form $E_{\text{out}}(\tau'_a) = \tilde{E}(z_a = L, \tau'_a)$ result in

$$\begin{aligned} A_{\text{out}}(\tau_{\text{lab}}) &= \frac{E_0}{2\pi} e^{-\delta_e L} \exp\{-ip \sin(\Omega\tau_{\text{lab}} + \vartheta_0)\} \\ &\times \sum_{n=-\infty}^{\infty} J_n(p) e^{i(\varphi_0 + n\vartheta_0)} \\ &\times \int_{-\infty}^{\infty} \frac{\exp\{-g(\omega)L - i\omega\tau_{\text{lab}}\}}{-i(\omega + n\Omega) + \Gamma_s/2} d\omega, \end{aligned} \quad (17)$$

where $\varphi_0' = \varphi_0 + \Delta\varphi_0$ and $\Delta\varphi_0 = i \frac{\omega_s}{c} L (\sqrt{\varepsilon} - 1)$.

The time-dependent probability of the photon detection behind the absorber can be described in terms of intensity of the output field, $N_{\text{out}}(\tau_{\text{lab}}) \propto I_{\text{out}}(\tau_{\text{lab}}) = \frac{c}{8\pi} |A_{\text{out}}(\tau_{\text{lab}})|^2$. From Eq. (17) we get

$$\begin{aligned} I_{\text{out}}(\tau_{\text{lab}}) &= \frac{I_0}{4\pi^2} e^{-T_e} \left| \sum_{n=-\infty}^{\infty} J_n(p) e^{in\vartheta_0} \right. \\ &\times \left. \int_{-\infty}^{\infty} \frac{\exp\{-g(\omega)L - i\omega\tau_{\text{lab}}\}}{-i(\omega + n\Omega) + \Gamma_s/2} d\omega \right|^2, \end{aligned} \quad (18)$$

where $I_0 = \frac{cE_0^2}{8\pi}$ is the peak intensity of the field of the incident photon (5a)–(5d) before transformation in the medium, and $T_e = 2\delta_e L$ is the exponent factor of photoelectric absorption. Thus, in the case under consideration, the optical depth of the resonant absorber at frequency ω is the sum of the resonant attenuation factor, $\text{Re}\{g(\omega)L\}$, specific for each frequency constituent, and the factor of photoelectric absorption, T_e , identical to all the constituents.

Let us note that an intensity of the field of the outgoing photon (the photon's waveform) in the laboratory reference frame (18) is the same as that in the reference frame of the oscillating absorber [see Eq. (15) and Fig. 1(b)], $I_{\text{out}}(\tau_{\text{lab}}) = I_{\text{out}}(\tau_a)$, since $|\exp\{\pm ip \sin(\Omega\tau_{\text{lab}} + \vartheta_0) - i\Delta\varphi_0\}|^2 = 1$. Using the vibrating reference frame allows one to considerably simplify the interpretation of changes in the photon waveform at the absorber exit.

III. ANALYTICAL STUDY

As follows from (1), (15), and (18), propagation of a photon through a vibrating absorber results in transformation of the slowly varying amplitude of the single-photon wave packet and the photon's waveform [Fig. 1(b), upper part]. This transformation can be interpreted in different ways. In the laboratory reference frame, it results from coherent forward scattering of the photon by the resonant nuclei with absorption or emission of acoustic phonons having the frequency of vibration. In the reference frame of the oscillating absorber, as seen from (9) and (15), this transformation originates from temporal interference of the frequency constituents of the multispiky continuous spectrum of the transmitted field. Analysis of such an intricate interference can be simplified if the relation (15) is represented as a superposition of the exponentially decaying spectral components with carrier frequencies $\omega_k = \omega_s + k\Omega$, the amplitudes of which acquire an additional temporal modulation owing to propagation through the resonant medium [Fig. 1(b), lower part]:

$$\begin{aligned} \tilde{E}(L, \tau_a) &= \theta(\tau_a) E_0 e^{i\varphi_0} e^{-T_e/2} e^{-\Gamma_s \tau_a/2} \\ &\times \sum_k A_k^{\text{DB}}(\tau_a) e^{-ik(\Omega\tau_a + \vartheta_0)}, \end{aligned} \quad (19a)$$

where using the solution from [23,28] one can write the time-dependent term $A_k^{\text{DB}}(\tau_a)$ of the k th outgoing spectral component as

$$A_k^{\text{DB}}(\tau_a) = J_{-k}(p) e^{-i\Delta\omega_k \tau_a} \sum_{n=0}^{\infty} \left(\frac{i\Delta\omega_k}{b} \right)^n (b\tau_a)^{\frac{n}{2}} J_n(2\sqrt{b\tau_a}), \quad (19b)$$

$\Delta\omega_k = \omega_a - \omega_s - k\Omega$, $b = \gamma_a T_M/2$, and $T_M = \frac{4\pi f_a n_{12} N |d_{12}|^2 \omega_a L}{\hbar c \sqrt{\epsilon} \gamma_a}$ is the Mössbauer thickness of the absorber. The temporal modulation of the slowly varying amplitude of an arbitrary k th spectral component (19b) is the well-known dynamical beats [23,24,26,29]. Its intensity,

$$\begin{aligned} I_k^{\text{DB}}(\tau_{\text{lab}}) &= \theta(\tau_{\text{lab}}) I_0 e^{-T_e} e^{-\Gamma_s \tau_{\text{lab}}} J_{-k}^2(p) \\ &\times \left| \sum_{n=0}^{\infty} \left(\frac{i\Delta\omega_k}{b} \right)^n (b\tau_a)^{\frac{n}{2}} J_n(2\sqrt{b\tau_a}) \right|^2, \end{aligned} \quad (19c)$$

was observed (in the case of absence of vibrations of both the source and absorber) for the first time in [23].

The dynamical beats of the k th spectral component arise from selective interaction of its frequency constituents with the absorber transition. Since the bandwidth of the component is comparable to the linewidth of the resonant transition, it is not absorbed as a whole. Instead, its spectrum is altered due to different influence of the resonant absorption and resonant dispersion on its frequency constituents [23,24,26,29]. Interference of the altered frequency constituents within the spectral contour results in dynamical beats of the k th component. They become quite visible if the bandwidth of the component is comparable to or larger than the linewidth of the resonant transition of an optically deep absorbing medium.

An alternative way to consider the output field in the vibrating reference frame (9), (15), and (19a) is to represent it in the form of a superposition of the incident field and resonant coherently forward-scattered field. Using (5) one can rewrite the slowly varying amplitude (15) and (19a) as

$$\begin{aligned} \tilde{E}(L, \tau_a) &= \theta(\tau_a) E_0 e^{i\varphi_0} e^{-T_e/2} e^{-\Gamma_s \tau_a/2} \\ &\times \sum_k \{ J_{-k}(p) + A_k^{\text{FS}}(\tau_a) \} e^{-ik(\Omega\tau_a + \vartheta_0)}. \end{aligned} \quad (19d)$$

Here the first term in curly brackets is the exponentially decaying spectral component with carrier frequency $\omega_k = \omega_s + k\Omega$ of the incident frequency-modulated field (5c) (accounting for the photoelectric absorption) and the second term is the resonant coherently forward-scattered field at the corresponding frequency. Comparing (19a) and (19d) one can write the time-dependent term $A_k^{\text{FS}}(\tau_a)$ of the k th forward-scattered-field component as

$$\begin{aligned} A_k^{\text{FS}}(\tau_a) &= A_k^{\text{DB}}(\tau_a) - J_{-k}(p) \\ &= J_{-k}(p) \left\{ e^{-i\Delta\omega_k \tau_a} \sum_{n=0}^{\infty} \left(\frac{i\Delta\omega_k}{b} \right)^n \right. \\ &\quad \left. \times (b\tau_a)^{\frac{n}{2}} J_n(2\sqrt{b\tau_a}) - 1 \right\}. \end{aligned} \quad (19e)$$

Similar to dynamical beats, the k th spectral component of the resonant forward-scattered field has the amplitude modulation caused by the temporal interference of its frequency constituents within the spectral profile.

The interference of frequency constituents within each spectral component (19c) or (19e) of the superposition (19a) or (19d) is accompanied by the temporal interference between the spectral components as a whole. In other words, the dynamical beats (19b) interfere with each other, while the coherently scattered-field components (19e) interfere both with each other and with the incident frequency-modulated field (4) and (5). Let us consider this interference in more detail in the case where the oscillation frequency is much larger than linewidths of the source and absorber, $\Omega \gg \Gamma_s, 2\gamma_a$, and the central frequency of some m th spectral component of the incident field in the oscillating reference frame (5a)–(5d), $\omega_m = \omega_s + m\Omega$ (where m is an integer number), is resonant to the frequency ω_a of transition $|1\rangle \leftrightarrow |2\rangle$ of the absorber, $\Delta\omega_m = 0$. Then similar to [20] one can assume that only the resonant m th spectral component interacts

with this transition, while the other spectral components experience only the nonresonant photoelectric absorption. In such a case one has $A_k^{\text{DB}}(\tau_a) = J_{-k}(p)$ and $A_k^{\text{FS}}(\tau_a) = 0$ for $k \neq m$, while $A_m^{\text{DB}}(\tau_a) = J_{-m}(p)J_0(2\sqrt{b\tau_a})$ and $A_m^{\text{FS}}(\tau_a) = J_{-m}(p)\{J_0(2\sqrt{b\tau_a}) - 1\}$. Thus the slowly varying amplitude of the output field in the oscillating reference frame (15) has a form of a superposition of the off-resonant spectral components transmitted without resonant interaction and the m th component, the amplitude of which constitutes the dynamical beats:

$$\tilde{E}(L, \tau_a) = \theta(\tau_a)E_0 e^{i\varphi_0} e^{-T_c/2} e^{-\Gamma_s \tau_a/2} \times \{A^{\text{pulse}}(\tau_a) + A_m^{\text{DB}}(\tau_a) e^{-im(\Omega\tau_a + \vartheta_0)}\}, \quad (20a)$$

$$A^{\text{pulse}}(\tau_a) = \sum_{n \neq -m} J_n(p) e^{in(\Omega\tau_a + \vartheta_0)} = e^{ip \sin(\Omega\tau_a + \vartheta_0)} - J_{-m}(p) e^{-im(\Omega\tau_a + \vartheta_0)}, \quad (20b)$$

$$A_m^{\text{DB}}(\tau_a) = J_{-m}(p) J_0(2\sqrt{b\tau_a}). \quad (20c)$$

According to (20), the time dependence of intensity of the output radiation (18) can be now expressed in the following form:

$$I_{\text{out}}(\tau_{\text{lab}}) = \theta(\tau_{\text{lab}}) I_0 e^{-T_c} e^{-\Gamma_s \tau_{\text{lab}}} \{ |A^{\text{pulse}}|^2 + |A_m^{\text{DB}}|^2 + 2\text{Re}(A^{\text{pulse}} A_m^{\text{DB}} e^{im(\Omega\tau_a + \vartheta_0)}) \}, \quad (21a)$$

where

$$|A^{\text{pulse}}|^2 = 1 + J_{-m}^2(p) - 2J_{-m}(p) \cos[p \sin(\Omega\tau_{\text{lab}} + \vartheta_0) + m(\Omega\tau_{\text{lab}} + \vartheta_0)], \quad (21b)$$

$$|A_m^{\text{DB}}|^2 = J_{-m}^2(p) J_0^2(2\sqrt{b\tau_{\text{lab}}}), \quad (21c)$$

$$2\text{Re}(A^{\text{pulse}} A_m^{\text{DB}} e^{im(\Omega\tau_a + \vartheta_0)}) = 2J_{-m} J_0(2\sqrt{b\tau_{\text{lab}}}) \{ \cos[p \sin(\Omega\tau_{\text{lab}} + \vartheta_0) + m(\Omega\tau_{\text{lab}} + \vartheta_0)] - J_{-m} \}. \quad (21d)$$

Equations (21a)–(21d) can be written in the equivalent compact form

$$I_{\text{out}}(\tau_{\text{lab}}) = \theta(\tau_{\text{lab}}) I_0 e^{-T_c} e^{-\Gamma_s \tau_{\text{lab}}} \{ 1 + J_{-m}^2(p) \times [J_0(2\sqrt{b\tau_{\text{lab}}}) - 1]^2 + 2J_{-m}(p) \times [J_0(2\sqrt{b\tau_{\text{lab}}}) - 1] \cos[p \sin(\Omega\tau_{\text{lab}} + \vartheta_0) + m(\Omega\tau_{\text{lab}} + \vartheta_0)] \}, \quad (21e)$$

which coincides with the result of [20].

As follows from Eqs. (20) and (21), both the slowly varying amplitude of the single-photon wave packet, $\tilde{E}(L, \tau_a)$, and the waveform of the photon, $I_{\text{out}}(\tau_{\text{lab}})$, transmitted through an optically deep vibrating absorber, acquire two types of amplitude modulation. The first type is described by formulas (20b) and (21b). It contributes into the total photon detection probability (21a) via relation (21b). This modulation is due to the absorber's vibration and was discussed in detail in [21]. Its origin can be explained as follows. At the entrance to the medium the spectrum of the photon 5(a)–5(d) in the

vibration reference frame constitutes a set of approximately $2p + 1$ equidistant spectral components separated by the frequency of oscillations. The amplitude of the n th component is determined by Bessel function $J_{-n}(p)$ of order $-n$. The central phase of the n th component is determined by a sign of the corresponding Bessel function, as well as by the phase term $n\vartheta_0 - \varphi_0$. Due to self-consistency of the incident spectrum, represented by the relation $J_{-n}(p) = (-1)^n J_n(p)$, the incident field (5) is frequency modulated and does not have any amplitude modulation apart from the exponential factor $\exp\{-\Gamma_s \tau_a/2\}$. Elimination of the resonant m th component as a whole, assumed in (20b), destroys the balance between the spectral components in the superposition. This results in appearance of amplitude modulation, which allows producing a train of short pulses under certain conditions [19–21]. Below, just such conditions providing formation of pulses are considered and hence this off-resonant part of the incident field is marked by the superscript “pulse.”

However, as discussed above, the resonant m th spectral component is not eliminated as a whole but comes out of the absorber being reduced and spectrally transformed. In the time domain its amplitude constitutes the dynamical beats described by the second term in (20a) [Fig. 1(b), green curve]. So, both the slowly varying amplitude of the single-photon wave packet (20a) and the waveform of the photon (21a) and (21e) are shaped also owing to dynamical beats of the resonant m th sideband described by formulas (20c) and (21c). According to (21a) and (21c), the waveform of dynamical beats of the resonant m th sideband can be written as

$$I_m^{\text{DB}}(\tau_{\text{lab}}) = \theta(\tau_{\text{lab}}) I_0 e^{-T_c} e^{-\Gamma_s \tau_{\text{lab}}} J_{-m}^2(p) J_0^2(2\sqrt{b\tau_{\text{lab}}}). \quad (22)$$

As follows from (22), the waveform of dynamical beats of the m th sideband constitutes a sequence of dips and humps in the time-dependent detection probability, $I_m(\tau_{\text{lab}})$. Timing of dips and humps of the dynamical beats is determined by zeros and extrema of Bessel function $J_0(2\sqrt{b\tau_{\text{lab}}})$, where $b = \gamma_a T_M/2$, and thus by Mössbauer thickness of the absorber. In the case of a small Mössbauer thickness, the first dip and hump are situated far on the tail of the waveform of the transmitted photon and are negligible. With increasing value of the Mössbauer thickness the dips and humps are shifted towards the front of the waveform and become quite visible.

The third term in (21a) represented by relation (21d) is due to interference of the dynamical beats with an amplitude modulation (pulses) caused by an absorber's vibration. This interference may be constructive or destructive subject to the phase relation between the fields constituting pulse(s) and dynamical beats at the exit from the absorber. This interference leads to increase or decrease of the pulse height. Timing of dynamical beats with respect to the front of the waveform is governed by Mössbauer thickness of the absorber, T_M , while position of the pulses produced via the absorber's vibration is determined by the initial phase of vibration, ϑ_0 . Therefore, the maximum amplitude of pulses can be achieved via the joint optimization of the parameters T_M and ϑ_0 as follows from the formulas for the interference term in (21d) and (21e). In the next section the optimization problem is studied analytically and numerically.

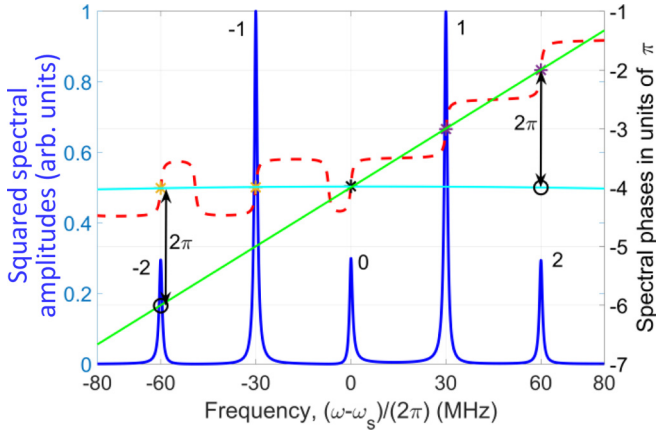


FIG. 2. Fourier transform of the incident photon field, emitted by the ^{57}Co radioactive source, in the reference frame of the oscillating ^{57}Fe absorber. The photon energy is $\hbar\omega_s = 14.4\text{ keV}$. The bandwidth of each sideband is $\Gamma_s/(2\pi) = 1.13\text{ MHz}$. The frequency of absorber's vibration is $\Omega/(2\pi) = 40\text{ MHz}$. The initial phase of vibration is $\vartheta_0 = 0$. The initial phase of the photon field is $\varphi_0 = 0$. The bold blue solid line corresponds to the squared modulus of the spectral amplitude of the field, while the bold dashed red line shows its spectral phase. The spectral phases at the central frequencies (central phases) of the (a) minus second and minus first, (b) zeroth, and (c) first and second spectral components are shown by (a) orange, (b) black, and (c) lavender asterisks, respectively. The central phases of the minus second and second sidebands, shifted by -2π , are shown by black circles. The central phases of the minus second, minus first, zeroth, and second spectral components are aligned along the light dash-dotted cyan horizontal line, while the central phases of the minus second, zeroth, first, and second spectral components are aligned along the light dash-dotted green diagonal line.

IV. OPTIMIZATION OF γ -RAY PULSE FORMATION VIA RESONANT SUPPRESSION OF THE PHASE-MISALIGNED SIDEBAND

Maximization of a pulse amplitude and minimization of pulse duration implies finding the optimal values of the following parameters: $\omega_a - \omega_s$, p , T_M , ϑ_0 , T_e , and Ω . As shown in [20,21], the quasimonochromatic photon field can be transformed into a regular train of pulses subject to $\omega_a - \omega_s = \pm\Omega$, i.e., via suppression of the \pm first ($m = \pm 1$) sideband of the photon field in the oscillating reference frame by tuning it to the absorber resonance (choosing $\Delta\omega_{-1} = 0$). It was shown also that maximizing amplitude of pulses is achieved in the case of maximization of the deleted sideband implemented at $p^{\text{opt}} \simeq 1.84$. These conditions have clear interpretation in the vibrating reference frame. In this case, the field of the incident photon consists of five spectral components with considerably nonzero amplitudes, namely, the minus second, minus first, zeroth, first, and second component [Figs. 1(b) and 2]. In the case of $\vartheta_0 = 0$ and $\varphi_0 = 0$, considered in Fig. 2, the central phases (the initial phases at the central frequencies) of the zeroth, minus first, and minus second components equal zero, while the central phases of the first and second sidebands equal π and 2π , respectively. Thus, the central phases of the minus second, minus first, zeroth, and second (phase 2π is equivalent to phase zero) spectral components are aligned along the horizontal line, while the central phases of the sec-

ond, first, zeroth, and minus second (phase zero is equivalent to phase -2π) spectral components are aligned along the inclined (diagonal) line. Such a phase alignment holds also in the case $\vartheta_0 \neq 0$ and $\varphi_0 \neq 0$ (when the n th spectral component acquires an additional phase shift $n\vartheta_0 + \varphi_0$). However, a nonzero value of ϑ_0 changes the slope of the lines, while a nonzero value of φ_0 shifts the lines as a whole in the vertical direction. Such a phase matching and specific amplitudes of the spectral components, proportional to $|J_n(p)|$, result in the absence of amplitude modulation of the incident photon field (4) and (5), apart from the exponential decay $\exp\{-\Gamma_s\tau_a/2\}$. Deletion of either the first or minus first sideband (assuming elimination of the sideband as a whole) via tuning it to the absorber resonance {by a proper choice of constant velocity V_s [Fig. 1(b)] of the source versus the absorber} destroys this balance and allows keeping only the phase-aligned components, the interference of which in the time domain leads to formation of a pulse train. If incomplete resonant absorption of the sideband is taken into account then the produced pulses interfere with the corresponding dynamical beats. As follows from Eqs. (20) and (21), transition from deletion of the first sideband to deletion of the minus first sideband shifts the pulses with respect to the front of the waveform by a half cycle of the absorber's vibration. So, for definiteness we shall consider the case of absorber resonance with the minus first sideband.

The optimal value of the modulation index can be explained in terms of the coherent forward-scattered field. According to (19d) and (19e) a resonant interaction of the minus first sideband with the absorber leads to the output field amplitude in the form $\tilde{E}(L, \tau_a) \propto e^{ip \sin(\Omega\tau_a + \vartheta_0)} + A_{-1}^{\text{FS}}(\tau_a) e^{i(\Omega\tau_a + \vartheta_0)}$, where the first term represents the incident frequency-modulated field (4) and (5) and $A_{-1}^{\text{FS}}(\tau_a) = -J_1(p)\{1 - J_0(2\sqrt{b\tau_a})\}$ is proportional to the amplitude of the appeared forward-scattered field. The forward-scattered field is fully coherent with the resonant minus first sideband and has the same carrier frequency. Temporal constructive interference of the forward-scattered field with the incident field leads to formation of pulses. The maximal pulse amplitude can be achieved subject to the maximal value of $A_{-1}^{\text{FS}}(\tau_a)$ which corresponds to maximization of $J_1(p)$ implemented at $p = p^{\text{opt}}$ where $J_1(p)$ is the normalized amplitude of the minus first sideband. Hence, maximizing the amplitude of the resonant first or minus first sideband of the incident field is the necessary condition for obtaining the highest pulse amplitude.

Let us find the values of T_M and ϑ_0 , maximizing the peak intensity of the produced pulses in the case where the modulation index is p^{opt} and the absorber is tuned to the resonance with the minus first sideband, $\Delta\omega_{-1} = 0$. First, let us consider the finite values of T_M and a small value of the ratio $\gamma_a/\Omega \ll 1$, such that only the resonant minus first sideband interacts with the absorber transition and the analytical results (20)–(22) are valid. The output photon waveform (21) is locally maximized (for arbitrary value of p), if $\cos[p \sin(\Omega\tau_{\text{lab}} + \vartheta_0) + m(\Omega\tau_{\text{lab}} + \vartheta_0)] = -1$. For $m = -1$ this corresponds to $p \sin(\Omega\tau_{\text{lab}} + \vartheta_0) - \Omega\tau_{\text{lab}} - \vartheta_0 = (2k+1)\pi$ and hence

$$\Omega\tau_{\text{lab}} + \vartheta_0 = (2k+1)\pi, \quad (23a)$$

where k is an integer number labeling the modulation peaks. Under the condition (23a), Eqs. (21) can be written in the form

$$I_{\text{out}}^{\text{peak}}(\tau_{\text{lab}}) = I_0 F_1(\tau_{\text{lab}}) F_2(\tau_{\text{lab}}), \quad (23b)$$

where

$$F_1(\tau_{\text{lab}}) = \theta(\tau_{\text{lab}}) e^{-T_e} e^{-\Gamma_s \tau_{\text{lab}}}, \quad (23c)$$

$$F_2(\tau_{\text{lab}}) = |A_{\text{max}}^{\text{pulse}}|^2 + |A_{-1}^{\text{DB}}|^2 + 2\text{Re}(A_{\text{max}}^{\text{pulse}} A_{-1}^{\text{DB}} e^{-i(\Omega\tau_a + \vartheta_0)}) \\ = \{1 + J_1(p)[1 - J_0(2\sqrt{b\tau_{\text{lab}}})]\}^2. \quad (23d)$$

It follows from (21) that

$$|A_{\text{max}}^{\text{pulse}}|^2 = [1 + J_1(p)]^2, \quad (24a)$$

$$|A_{-1}^{\text{DB}}|^2 = J_1^2(p) J_0^2(2\sqrt{b\tau_{\text{lab}}}), \quad (24b)$$

$$2\text{Re}(A_{\text{max}}^{\text{pulse}} A_{-1}^{\text{DB}} e^{-i(\Omega\tau_a + \vartheta_0)}) = -2J_1(p) J_0(2\sqrt{b\tau_{\text{lab}}}) \\ \times [1 + J_1(p)]. \quad (24c)$$

At $p = p^{\text{opt}}$ local maxima are peaks of pulses, so that Eqs. (23) and (24) describe the time dependence of the peak intensity of the pulses. The function $F_1(\tau_{\text{lab}})$ is the waveform of the incident photon attenuated as a whole by the photoelectric absorption only. It has maximum, $F_1^{\text{max}} = 1$, at $T_e = 0$ and $\tau_{\text{lab}} = 0$. The function $F_2(\tau_{\text{lab}})$ determines the value of pulse peaks over $F_1(\tau_{\text{lab}})$ accounting for interference of pulses due to vibration with dynamical beats of the minus first component. As follows from (23d) and (24), if interference is absent or negligible [$J_0(2\sqrt{b\tau_{\text{lab}}}) = 0$ or $J_0(2\sqrt{b\tau_{\text{lab}}}) \ll 1$ occurred in deeps of dynamical beats or if $b\tau_{\text{lab}} \gg 1$, respectively], then $F_2(\tau_{\text{lab}}) \simeq 2.5$. The function $F_2(\tau_{\text{lab}})$ takes the maximum value, $F_2(\tau_{\text{lab}}) = F_2^{\text{max}} \simeq 3.3$, when the minimum of $J_0(2\sqrt{b\tau_{\text{lab}}}) \simeq -0.4$ is achieved at $2\sqrt{b\tau_{\text{lab}}} \simeq 3.8$. This occurs at the first hump of dynamical beats (21c), (22), and (24b) resulting in a maximum constructive interference between the pulses (20b) and dynamical beats (20c). Maximization of the interference term (24c) gives the largest enhancement in pulse amplitude, $2\text{Re}(A_{\text{max}}^{\text{pulse}} A_{-1}^{\text{DB}} e^{-i(\Omega\tau_a + \vartheta_0)})_{\text{max}} \simeq 0.7$. On the other hand, if some pulse peak coincides with the second hump of dynamical beats (21c), (22), and (24b) corresponding to the first local maximum of $J_0(2\sqrt{b\tau_{\text{lab}}}) \simeq 0.3$, achieved at $2\sqrt{b\tau_{\text{lab}}} \simeq 7$, the maximum destructive interference (minimum value of the interference term (24c), $2\text{Re}(A_{\text{max}}^{\text{pulse}} A_{-1}^{\text{DB}} e^{-i(\Omega\tau_a + \vartheta_0)})_{\text{min}} \simeq -0.6$) between the pulses (20b) and dynamical beats (20c), occurs. In this case dynamical beats reduce the pulse amplitude resulting in $F_2(\tau_{\text{lab}}) = F_2^{\text{min}} \simeq 1.98$.

In order to maximize the product $F_1(\tau_{\text{lab}})F_2(\tau_{\text{lab}})$ one should simultaneously maximize Mössbauer thickness (in order to reduce τ_{lab} in the exponent $e^{-\Gamma_s \tau_{\text{lab}}}$ keeping unchanged the optimal value of $2\sqrt{b\tau_{\text{lab}}} = \sqrt{2\gamma_a T_M \tau_{\text{lab}}}$) and minimize T_e . However, T_e is proportional to T_M and is ultimately determined by the percentage of the resonant nuclei: the higher percentage of the resonant nuclei, the smaller physical thickness L of the absorber and, hence, the smaller photoelectric attenuation. Hence minimization of T_e can be done via enrichment of the absorber with the resonant nuclei. Similar to [19], we assume that ^{57}Fe nuclei are embedded into stainless steel which is a compound Fe:Cr:Ni at 70:19:11 wt. %. However, unlike [19] where the natural abundance $\sim 2.2\%$ of ^{57}Fe in

iron fraction was used, in order to minimize T_e , we assume the commercially available 90% enrichment of iron fraction by nuclide ^{57}Fe with natural broadening of the spectral line of the resonant transition, implying $\gamma_a = \Gamma_s/2$ and $2\sqrt{b\tau_{\text{lab}}} = \sqrt{T_M \Gamma_s \tau_{\text{lab}}}$. Taking into account that the photoelectric absorption coefficient in stainless steel is $5.06 \times 10^4 \text{ m}^{-1} < 2\delta_e < 5.17 \times 10^4 \text{ m}^{-1}$ [30], we get $T_e \simeq T_M/180$. Let us maximize Eq. (23b) for the above parameter values. Finding the partial derivatives of $I_{\text{out}}^{\text{peak}}$ over τ_{lab} and T_M , and equating them to zero after some transformations, we get

$$J_1(p^{\text{opt}}) \frac{J_1(\sqrt{T_M \Gamma_s \tau_{\text{lab}}})}{\sqrt{T_M \Gamma_s \tau_{\text{lab}}}} \\ = \frac{1}{T_M} \{1 + J_1(p^{\text{opt}})[1 - J_0(\sqrt{T_M \Gamma_s \tau_{\text{lab}}})]\}, \quad (25a)$$

$$\{1 + J_1(p^{\text{opt}})[1 - J_0(\sqrt{T_M \Gamma_s \tau_{\text{lab}}})]\}(\Gamma_s \tau_{\text{lab}} - T_M/180) \\ = 0. \quad (25b)$$

Equation (25b) has a solution $T_M = 180\Gamma_s \tau_{\text{lab}}$. Substituting it into Eq. (25a) we find

$$J_0(13.42\Gamma_s \tau_{\text{lab}}) + 13.42J_1(13.42\Gamma_s \tau_{\text{lab}}) - 2.719 = 0. \quad (25c)$$

The roots of this equation are $\Gamma_s \tau_{\text{lab}} \simeq [0.02; 0.24; 0.58; 0.69; 1.08; 1.12]$. The respective values of absorber Mössbauer thickness are $T_M \simeq [3.5; 44; 103.6; 123.8; 195.1; 201.6]$. According to (23), these values of $\Gamma_s \tau_{\text{lab}}$ and T_M correspond to the following values of the peak pulse intensity: $I_{\text{out}}^{\text{peak}}/I_0 \simeq [0.98; 1.94; 0.66; 0.70; 0.27; 0.27]$. Thus, the largest maximum, $\text{Max}\{I_{\text{out}}^{\text{peak}}/I_0\} \simeq 1.94$, of pulse height is achieved at $\Gamma_s \tau_{\text{lab}}^{\text{opt}} \simeq 0.24$ and $T_M^{\text{opt}} \simeq 44$, corresponding to the physical thickness of the film $L \simeq 4.8 \mu\text{m}$. The respective optimal values of the initial phase of vibration are $\vartheta_0^{\text{opt}} \simeq (2k+1)\pi - 0.24\Omega/\Gamma_s$. The waveform corresponding to these optimal parameter values is plotted in Fig. 3 for $\gamma_a/\Omega \simeq 5.8 \times 10^{-4}$. In this case, according to (23c), one has $F_1(\tau_{\text{lab}}) = 0.78\theta(\tau_{\text{lab}})e^{-\Gamma_s \tau_{\text{lab}}}$, where $\theta(\tau_{\text{lab}})e^{-\Gamma_s \tau_{\text{lab}}}$ is the waveform of the incident photon represented by the black dashed curve in Fig. 3. It can be seen that because of the exponential dependence of $F_1(\tau_{\text{lab}})$ the value $\text{Max}\{I_{\text{out}}^{\text{peak}}/I_0\} \simeq 1.94$ is achieved slightly earlier, at $2\sqrt{b\tau_{\text{lab}}} \simeq 3.3$, than the first hump of dynamical beats, which occurred at $2\sqrt{b\tau_{\text{lab}}} \simeq 3.8$. For $T_M^{\text{opt}} \simeq 44$ the respective times are $\tau_{\text{lab}} \simeq 35\text{ns}$ for the maximum of pulse height and $\tau_{\text{lab}} \simeq 46\text{ns}$ for the first hump of dynamical beats.

The accuracy of obtained analytical results decreases with increasing value of γ_a/Ω . This is because the other spectral components of the photon field are also influenced by the resonant absorption and primarily by the resonant dispersion, which lead to (i) change of central phases of the spectral components and (ii) distortion of amplitudes and primarily phases of Fourier constituents within the spectral contour of each component. As a result, the exact solution for the waveform of the output photon (18) and the corresponding optimal values of $\Gamma_s \tau_{\text{lab}}$ and T_M deviate from the results of the analytical study.

Let us trace the dependence of these deviations as a function of the frequency of the absorber's vibration. In

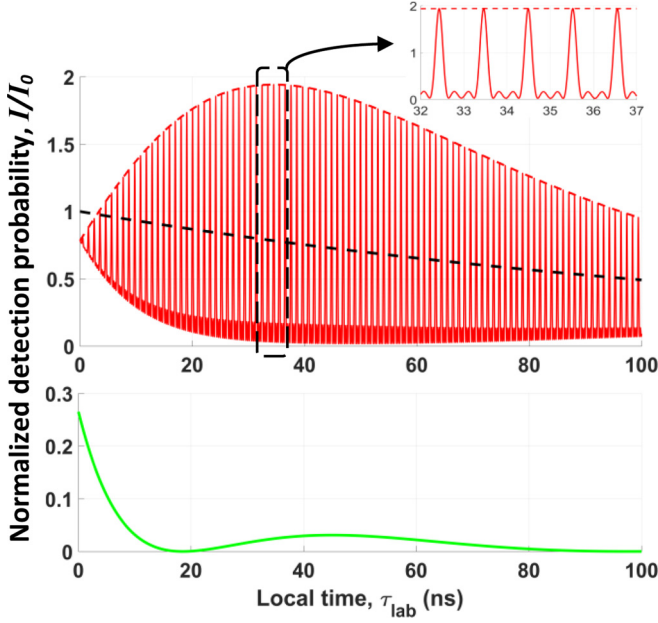


FIG. 3. Time dependence of the photon detection probability, $I_{\text{out}}(\tau_{\text{lab}})$, normalized to the peak detection probability of the photon at the absorber entrance, I_0 (red pulses), for the vibration frequency 970 MHz corresponding to the analytical solution (21) that in this case practically coincides with general solution (18) at this vibration frequency. Tops of pulses are described by relation (23a). The red dashed curve is the pulse envelope, $I_{\text{out}}^{\text{peak}}(\tau_{\text{lab}})$, Eq. (23). The black dashed curve is the waveform of the incident photon. The green curve in the lower panel represents the dynamical beats of the minus first sideband of the photon field (in the vibrating reference frame) plotted according to Eq. (22) for $m = -1$. Pulse duration is about 190 ps. The maximum of pulse height and the first hump of dynamical beats occur at $\tau_{\text{lab}} \cong 35$ and 46 ns, respectively.

Figs. 4(a) and 4(b) we show the optimal values of (a) Mössbauer thickness, $T_M^{\text{opt}}(\Omega)$, and (b) the moment of formation of the pulse with the highest intensity, $\tau_{\text{lab}}^{\text{opt}}(\Omega)$, found via the numerical analysis of Eq. (18), versus the frequency of vibration. Figure 4(c) shows the frequency dependence of maximum intensity of the highest pulse (maximum of the peak detection probability), $\text{Max}\{I(\tau_{\text{lab}})/I_0\} = I_{\text{out}}^{\text{peak}}(T_M^{\text{opt}}(\Omega), \tau_{\text{lab}}^{\text{opt}}(\Omega), \vartheta_0^{\text{opt}}(\Omega))/I_0 = I_{\text{max}}(\Omega)/I_0$. In Figs. 4(a)–4(c) the numerical results are compared with the analytical solution. As can be seen, at high frequencies of vibration, $\Omega/(2\pi) > 150$ MHz, the results of numerical optimization and the analytical solution almost coincide. This means that the maximum of the peak detection probability practically does not depend on the vibration frequency and is $I_{\text{max}}/I_0 \cong 1.94$ as has been found within the analytical model. This value is achieved at $\tau_{\text{lab}}^{\text{opt}} \cong 35$ ns and can be implemented with an absorber of Mössbauer thickness $T_M^{\text{opt}} \cong 44$ irrespective of the vibration frequency. This is because at such vibration frequencies and Mössbauer thickness only the minus first spectral component of the photon field is really altered during propagation through the absorber. As shown in [19], the pulse repetition rate equals the vibration frequency and pulse duration is defined by inverse of the product of the number of phase-aligned components and the

vibration frequency. Therefore the shortest pulse duration that could be produced by the discussed technique is limited by the highest available vibration frequency of the piezoelectric transducer with the desired amplitude and linewidth. The maximum frequency of the diamond piezoelectric transducer is 970 MHz [31]. In this case the regular pulse sequence shown in Fig. 3 can be produced with pulse duration of about 190 ps. The polyvinylidene fluoride piezoelectric transducers operating at frequencies up to 24 GHz [32] allows producing pulses to 7.7 ps.

At frequencies below 150 MHz the discrepancy between the analytical and numerical results increases as the frequency decreases, reaching a maximum at the lowest considered vibration frequency (Fig. 4). This is caused by increasing influence of nuclear transition on the off-resonant spectral components of the photon field. At the considered vibration frequencies $\Omega/\Gamma_s \geq 10$ one can neglect the resonant absorption of the off-resonant spectral components. However, the resonant dispersion can noticeably modify the phase relations both between the frequency constituents within each off-resonant spectral component and between central phases of spectral components owing to their different phase incursion during propagation through the medium. According to (13b) and (14), the phase incursion of an arbitrary frequency constituent of the photon field with frequency ω at the absorber exit is $\Phi(\omega) = \text{Im}\{g(\omega)L\} = \frac{T_M \gamma_a}{2} \frac{(\omega_a - \omega_s - \omega)}{\gamma_a^2 + (\omega_a - \omega_s - \omega)^2}$. This means that, for instance, the phase misalignment at central frequencies of the closest to nuclear transition minus second and zeroth components behind the absorber is $\Delta\Phi_{-2,0} = \Phi(-2\Omega) - \Phi(0) \cong \Gamma_s T_M / (2\Omega)$. At $\Gamma_s / (2\pi) = 1$ MHz, $\Omega / (2\pi) = 10$ MHz, and $T_M^{\text{opt}} = 20$ [the first circle in Figs. 4(a)–4(c)] the phase misalignment is $\Delta\Phi_{-2,0} \cong \pi/3$. Such phase distortions noticeably change the temporal interference pattern; optimal values of T_M^{opt} , ϑ_0^{opt} , and $\tau_{\text{lab}}^{\text{opt}}$; as well as the highest peak pulse intensity I_{max}/I_0 (Fig. 4; the difference in pulse shape is quite visible in Figs. 3, 7, and 8). The changes in the temporal interference pattern are taken into account in relations (19) and (20). They can be interpreted via generation of the off-resonant spectral components of the forward-scattered field with time-dependent amplitudes (19d), and the temporal interference of the forward-scattered-field components with both pulses and dynamical beats of the minus first spectral component (20) as follows:

$$\begin{aligned} \tilde{E}(L, \tau_a) = & \theta(\tau_a) E_0 e^{i\varphi_0} e^{-T_e/2} e^{-\Gamma_s \tau_a/2} \\ & \times \left\{ A^{\text{pulse}}(\tau_a) + A_{-1}^{\text{DB}}(\tau_a) e^{-i(\Omega\tau_a + \vartheta_0)} \right. \\ & \left. + \sum_{k \neq -1} A_k^{\text{FS}}(\tau_a) e^{-ik(\Omega\tau_a + \vartheta_0)} \right\}. \end{aligned} \quad (26)$$

As shown in Fig. 4, for every vibration frequency there is some optimal Mössbauer thickness, T_M^{opt} , and initial vibration phase, ϑ_0^{opt} , at which the constructive interference of the terms in (26) results in the highest peak pulse intensity I_{max}/I_0 at the corresponding moment $\tau_{\text{lab}}^{\text{opt}}$. At vibration frequencies $\Omega/(2\pi) < 18$ MHz large distortions of the output spectral components, caused by the off-resonant

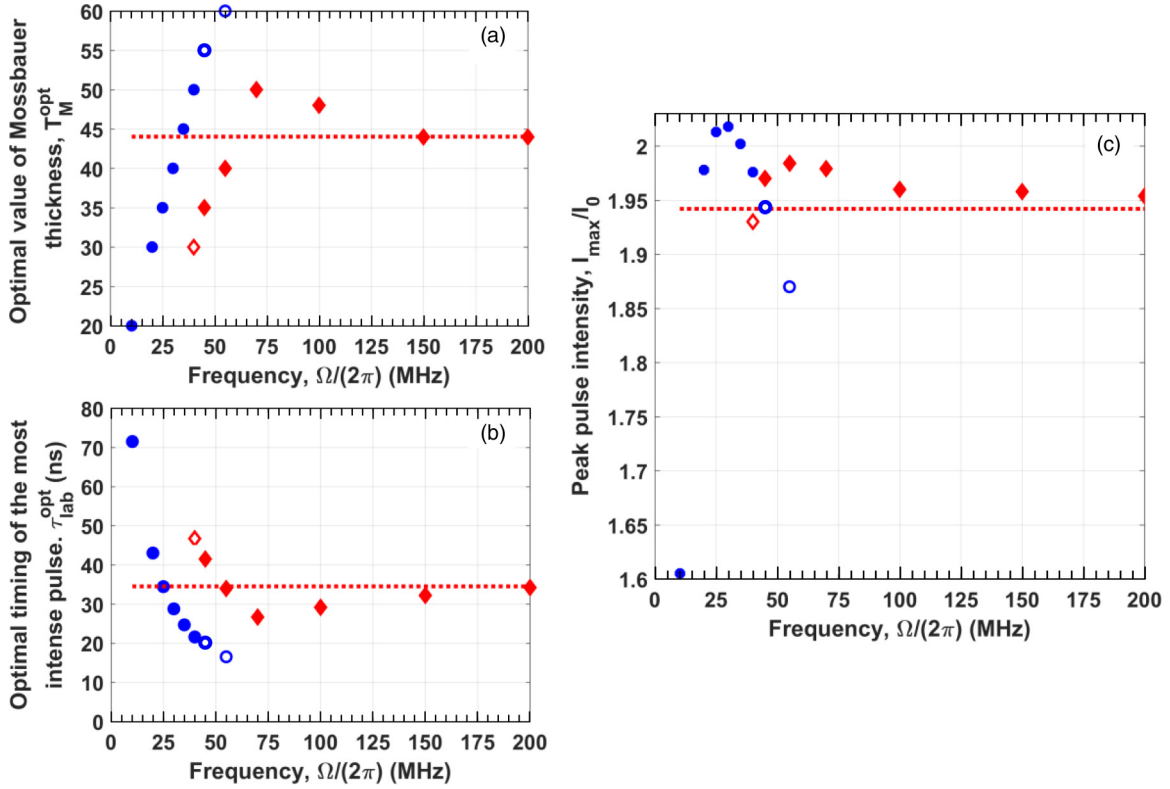


FIG. 4. Vibration frequency dependencies of the optimal values of (a) Mössbauer thickness of the absorber, $T_M^{\text{opt}}(\Omega)$, and (b) the moment of formation of the highest pulse, $\tau_{\text{lab}}^{\text{opt}}(\Omega)$, as well as (c) the corresponding intensity of the highest pulse, $I_{\text{max}}(\Omega)/I_0$, shown by filled marks at discrete frequency values with step multiples of 5 MHz. Blue and red filled and open marks are numerical optimizations of Eq. (18) the red dotted line is optimization (25) of the analytical solution (23). At $\Omega/(2\pi) = 40, 45, 55$ MHz two values, T_M^{opt} and T_M' in (a) as well as $\tau_{\text{lab}}^{\text{opt}}$ and τ_{lab}' in (b), are shown by filled and open marks, respectively. These values correspond to the maximum peak pulse intensity, I_{max}/I_0 [the respective filled marks in (c)] and to the lower maximum, I_{max}'/I_0 [the respective open marks in (c)] which appears at frequency $\Omega/(2\pi) \simeq 35$ MHz and disappears at $\Omega/(2\pi) \simeq 75$ MHz (having values out of the displayed region). For example, at frequency $\Omega/(2\pi) = 45$ MHz the first (from the left) filled red rhombs in (a) and (b) label values $T_M^{\text{opt}} \simeq 35$ and $\tau_{\text{lab}}^{\text{opt}} \simeq 41.5$ ns, respectively, corresponding at this frequency to the maximum peak pulse intensity $I_{\text{max}}/I_0 \simeq 1.97$ [also labeled by the filled red rhomb in (c)]. The lower value, $I_{\text{max}}'/I_0 \simeq 1.94$, in (c) corresponds to $T_M' \simeq 55$ in (a) and $\tau_{\text{lab}}' \simeq 20$ ns in (b) and is labeled by open circles. More detailed discussion is given in the text and in Fig. 5(b).

forward-scattered field, hamper pulse formation via resonant absorption of the minus first component; I_{max}/I_0 is less than that followed from the analytical model neglecting the off-resonant forward-scattered field [Fig. 4(c)]. As the vibration frequency growth, the phase misalignment at optimal conditions becomes smaller in spite of increasing optimal Mössbauer thickness [for example, at $\Omega/(2\pi) = 30$ MHz and $T_M^{\text{opt}} = 40$ the phase misalignment is $\Delta\Phi_{-2,0} \simeq \pi/5$]. Moreover, at $\Omega/(2\pi) > 18$ MHz contribution of the off-resonant forward-scattered field at the moment $\tau_{\text{lab}}^{\text{opt}}$ becomes constructive leading to enhancement in peak pulse intensity; I_{max}/I_0 becomes larger than that followed from the analytical model [Fig. 4(c)]. At vibration frequency $\Omega/(2\pi) \simeq 30$ MHz the constructive interference of all the transmitted frequency constituents [of all the terms in (26)] results in a global maximum of photon peak detection probability, $I_{\text{max}}^{\text{Glob}}/I_0 \simeq 2.02$, that occurs at $\tau_{\text{lab}}^{\text{Glob}} \simeq 28$ ns and $\vartheta_0^{\text{Glob}} \simeq 5\pi/4$ upon $T_M^{\text{Glob}} \simeq 40$. It should be mentioned that the optimal quite high Mössbauer thickness, $T_M^{\text{Glob}} \simeq 40$, is experimentally feasible since it corresponds to the physical thickness of the stainless steel film $L \simeq 4.4 \mu\text{m}$. This global maximum is shown in Fig. 5(a) by a gray spot at the coordinate plane of the Mössbauer thickness,

T_M , and the initial phase of the absorber's vibration, ϑ_0 . As can be seen, deviation of either T_M or ϑ_0 from their optimal values results in decrease of the peak detection probability, $I_{\text{out}}^{\text{peak}}(T_M, \tau_{\text{lab}}^*, \vartheta_0) < I_{\text{max}}^{\text{Glob}}/I_0$ [where $\tau_{\text{lab}}^* \equiv \tau_{\text{lab}}(T_M, \vartheta_0)$ corresponds to the top of the highest pulse], because of violation of the constructive interference condition.

A dependence of the peak detection probability on the absorber's Mössbauer thickness and initial phase of vibration qualitatively similar to the one displayed in Fig. 5(a) could be plotted also in the above discussed case of high vibration frequency, $\Omega/(2\pi) > 150$ MHz, where contribution of the phase distortion is negligible, while the constructive interference between the vibrationally induced pulses and dynamical beats of the minus first spectral component would provide the largest value of $I_{\text{out}}^{\text{peak}}(T_M, \tau_{\text{lab}}^*, \vartheta_0)$ at $T_M \rightarrow \infty$ and $\tau_{\text{lab}}^* \rightarrow 0$. This is because at $T_M < T_M^{\text{opt}}$ the insufficiently attenuated resonant minus first sideband of the photon field spoils the pulse formation. At $T_M > T_M^{\text{opt}}$ the minus first sideband is attenuated more strongly. As a result, constructive interference of the remaining in-phase components leads to formation of the pulses with higher amplitude. However, with increasing T_M the nonresonant photoelectric absorption coefficient T_e

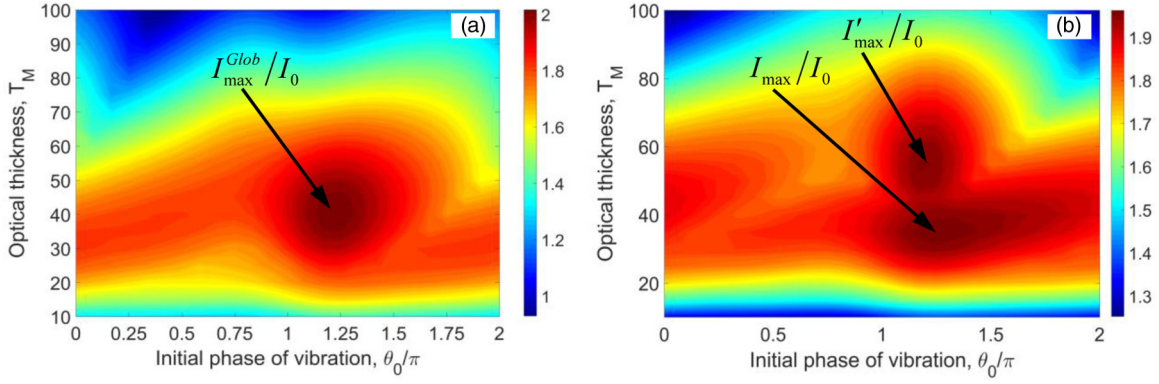


FIG. 5. Peak detection probability of the photon, normalized to peak detection probability at the absorber entrance, $I_{\text{out}}^{\text{peak}}(T_M, \tau_{\text{lab}}^*, \vartheta_0)/I_0$ [where $\tau_{\text{lab}}^* \equiv \tau_{\text{lab}}(T_M, \vartheta_0)$ corresponds to the top of the highest pulse], vs the Mössbauer thickness, T_M , and the initial phase of the absorber's vibration, ϑ_0 , at the determined value of Ω . The calculations are based on Eq. (18) where the minus first sideband of the photon field is tuned to the resonance ($m = -1$ and $\omega_s - \omega_a = \Omega$). The frequency of vibration is $\Omega/(2\pi) = 30$ MHz for (a) and $\Omega/(2\pi) = 45$ MHz for (b). The maximum value for (a) is $I_{\text{max}}^{\text{Glob}}/I_0 \simeq 2.02$ achieved at $T_M^{\text{Glob}} \simeq 40$, $\vartheta_0^{\text{Glob}} \simeq 5\pi/4$, and $\tau_{\text{lab}}^* = \tau_{\text{lab}}^{\text{Glob}} \simeq 28$ ns. In the case (b) there are two maxima: $I_{\text{out}}^{\text{peak}}(T_M, \tau_{\text{lab}}^*, \vartheta_0)/I_0 = I_{\text{max}}/I_0 \simeq 1.97$ [see also Fig. 4(c), the first filled red rhomb] is achieved at $T_M = T_M^{\text{opt}} \simeq 35$ [see also Fig. 4(a), the first filled red rhomb], $\vartheta_0 \simeq 5\pi/4$, and $\tau_{\text{lab}}^* = \tau_{\text{lab}}^{\text{opt}} \simeq 41.5$ ns [see also Fig. 4(b), the first filled red rhomb]; as well as $I_{\text{out}}^{\text{peak}}(T_M, \tau_{\text{lab}}^*, \vartheta_0)/I_0 = I'_{\text{max}}/I_0 \simeq 1.94$ [see also Fig. 4(c), the first open circle], achieved at $T_M = T'_M \simeq 55$ [see also Fig. 4(a), the first open circle], $\vartheta_0 \simeq 5\pi/4$, and $\tau_{\text{lab}}^* = \tau'_{\text{lab}} \simeq 20$ ns [see also Fig. 4(b), the first open circle].

also grows (in the considered case $T_e = T_M/180$), leading to attenuation of the photon field as a whole and reduction of the output photon detection probability. The photoelectric attenuation plays the major role in formation of maximum photon detection probability at relatively low percentage of the resonant nuclei, i.e., upon the condition $\Gamma_s T_M/\Omega \ll T_e$. Otherwise (including the case $T_e = 0$) the above discussed interference cannot be neglected.

The temporal interference plays the major role in formation of ‘‘jump’’ in dependences of $T_M^{\text{opt}}(\Omega)$ and $\tau_{\text{lab}}^{\text{opt}}(\Omega)$, as well as a kink of function $I_{\text{max}}(\Omega)/I_0$ at $40 \text{ MHz} < \Omega/(2\pi) < 45 \text{ MHz}$ (Fig. 4). As can be seen from Fig. 4(c), starting from frequency $\Omega/(2\pi) \simeq 35$ MHz, the temporal interference between the frequency constituents of the outgoing field (26) is able to produce at the same vibration frequency Ω two maxima, I_{max}/I_0 (filled marks) and I'_{max}/I_0 (open marks) in the peak detection probability of the output field achieved at the corresponding values T_M^{opt} and T'_M [filled and open marks, respectively, in Fig. 4(a)] as well as $\tau_{\text{lab}}^{\text{opt}}$ and τ'_{lab} [filled and open marks, respectively, in Fig. 4(b)]. This is illustrated in Fig. 5(b) for $\Omega/(2\pi) \simeq 45$ MHz by two gray spots situated at larger Mössbauer thickness [corresponding to earlier instant τ'_{lab} (open blue circle) in Fig. 4(b)] and at smaller Mössbauer thickness [corresponding to later instant $\tau_{\text{lab}}^{\text{opt}}$ (filled red rhomb) in Fig. 4(b)]. At $35 \text{ MHz} < \Omega/(2\pi) < 45 \text{ MHz}$ one has $I_{\text{max}} > I'_{\text{max}}$ under $T_M^{\text{opt}} > T'_M$ and $\tau_{\text{lab}}^{\text{opt}} < \tau'_{\text{lab}}$ [filled circles and open rhombs in Figs. 4(a)–4(c), respectively]. However, maximum peak detection probability decreases with increasing vibration frequency. At the same time, the second maximum in the peak detection probability, achieved at smaller Mössbauer thickness and later times (red open rhombs in Fig. 4), grows. Starting from vibration frequency $\Omega/(2\pi) \simeq 45$ MHz, smaller Mössbauer thickness and later moments provide a larger value of peak detection probability and become optimal (open rhombs become filled

rhombs). At frequencies $\Omega/(2\pi) > 75$ MHz the maximum in peak detection probability at high Mössbauer thickness and early times disappears. At the coordinate plane of the Mössbauer thickness, T_M , and the initial phase of the absorber's vibration, ϑ_0 , the peak detection probability at this frequency range has a similar look with a single gray spot as in the case $\Omega/(2\pi) < 35$ MHz displayed in Fig. 5(a).

The spectrum of the output photon field in the oscillating reference frame under the most optimal conditions providing the highest peak detection probability, $I_{\text{max}}^{\text{Glob}}/I_0 \simeq 2.02$, at $\Omega/(2\pi) = 30$ MHz, $T_M^{\text{Glob}} = 40$, and $\vartheta_0^{\text{Glob}} = 5\pi/4$, is shown in Fig. 6. The minus first sideband is almost fully absorbed (except for the spectral wings corresponding to dynamical beats in time representation), and only the phase-aligned

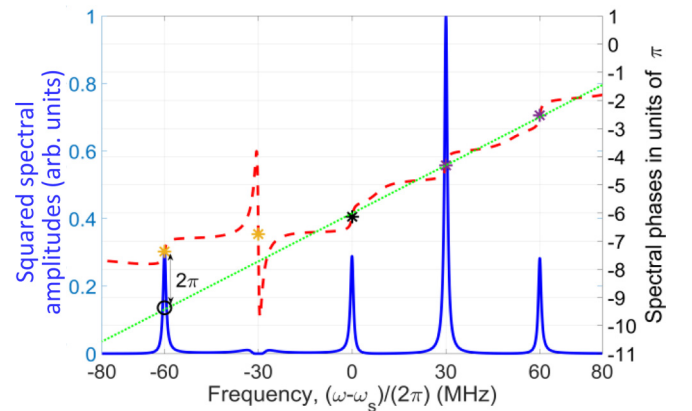


FIG. 6. The same as in Fig. 2, but after transmission of the photon through the resonant absorber tuned to the resonance with the minus first sideband of the photon field, under the global optimum conditions: $I_{\text{max}}^{\text{Glob}}/I_0 \simeq 2.02$, $\Omega/(2\pi) = 30$ MHz, $T_M^{\text{Glob}} = 40$, and $\vartheta_0^{\text{Glob}} = 5\pi/4$. The spectrum corresponds to blue curve in Fig. 7.

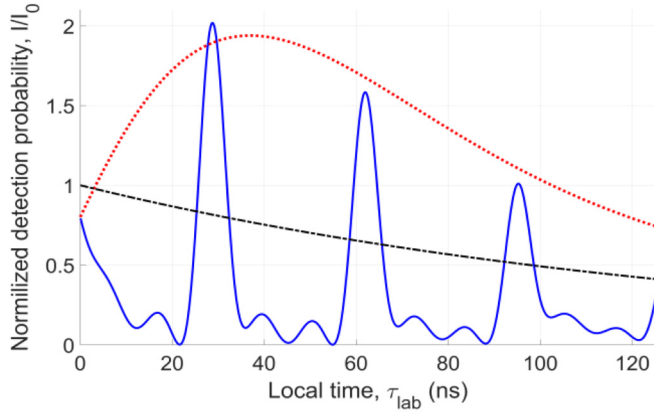


FIG. 7. Time dependence of the photon detection probability normalized to the peak detection probability of the photon at the absorber entrance, I_0 , corresponding to the spectrum in Fig. 6. The blue solid curve shows the general solution (18). Pulse duration is about 6 ns. The black dash-dotted curve is the waveform of the incident photon. The red dotted curve shows the analytical solution for the pulse envelope (23) at the same parameter values but accounting for the dynamical beats of the minus first sideband only.

minus second, zeroth, first, and second spectral components remain. However, the spectral phase of the field (shown by the red dashed curve) is noticeably distorted with respect to that in Fig. 2 due to interaction of nonresonant components with the absorber transition. The central phases of the minus second and zeroth components are shifted at $\pm\pi/5$ from their input values. In the time domain interference of the remaining spectral components of the photon field leads to formation of the pulse train shown in Fig. 7 with the highest peak detection probability, $I_{\max}^{\text{Glob}}/I_0 \simeq 2.02$. For chosen vibration frequency the duration of the first pulse is about 6 ns. The black dash-dotted curve shows the waveform of the photon at the absorber entrance and clearly demonstrates that although the photon field undergoes both resonant and photoelectric absorption the peak detection probability of the transmitted photon is more than two times higher than the peak detection probability at the absorber entrance. The red dotted curve, plotted according to Eqs. (23), traces the pulse height versus time, τ_{lab} , at the same parameter values ($p = p^{\text{opt}}$, $T_M = T_M^{\text{Glob}}$) accounting for the dynamical beats of the minus first sideband only. Its maximum indicates the highest detection probability under that approximation. It can be seen that taking into account the off-resonant spectral components of the forward-scattered field and their temporal interference with both pulses due to vibration and dynamical beats of the minus first component leads to increase in the highest detection probability and its shift towards the photon's front edge.

The numerically plotted pulses [according to exact formula (18)] and the curve [plotted according to approximate formulas (23)] roughly tracing their peaks (blue and red lines in Fig. 7) allow one to track the periodic dependence of peak detection probability of the photon on the initial phase of the absorber's vibration, shown in Fig. 5. In accordance with the analytical solution, the optimal value of the initial phase of vibration is $\vartheta_0^{\text{opt}} = (2k + 1)\pi - 0.24\Omega/\Gamma_s$ (where k is an integer number). At this value of ϑ_0 the respective

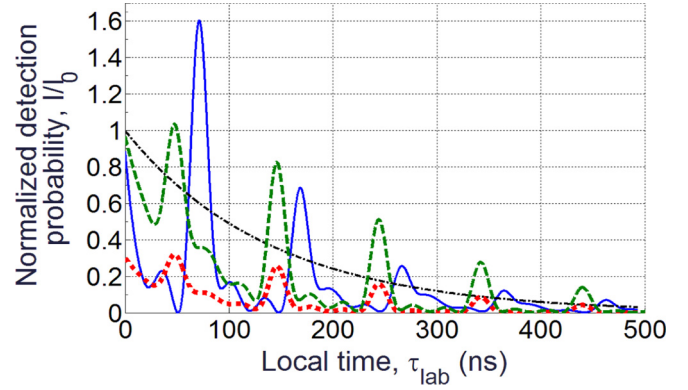


FIG. 8. Time dependence of detection probability of the γ -ray photon transmitted through vibrating stainless steel foil. The frequency of vibration for all curves is $\Omega/(2\pi) = 10.2$ MHz. The red dotted curve corresponds to the parameter values used in the experiment [19]: $T_M = 5.2$, $\vartheta_0 = 0$, natural abundance, 2.2%, of ^{57}Fe in iron fraction. The green dashed curve is plotted at the same parameter values but for 90% of ^{57}Fe in iron fraction. The blue solid curve is the result of optimization: 90% of ^{57}Fe in iron fraction, $T_M = 17.5$, $\vartheta_0 = 1.35\pi$. The absorber is tuned to resonance with the minus first sideband of the photon field in the oscillating reference frame. The black dash-dotted curve is the waveform of the photon at the absorber entrance.

k th pulse from the produced pulse train (21), centered at $\tau_{\text{lab}} = ([2k + 1]\pi - \vartheta_0^{\text{opt}})/\Omega$, is tuned to the maximum of the envelope (23). Deviation of the initial phase of vibration from its optimal value leads to a shift of the position of the k th pulse from the maximum of the envelope, and reduction of its intensity. However, whether the k th pulse is shifted to the right or to the left, a neighboring (either $k-1$ or $k+1$) pulse moves towards the peak of the envelope, and after a 2π shift of the initial phase of vibration it occupies the optimal position.

In order to illustrate the effect of joint optimization of the absorber optical depth and the initial oscillation phase, in Fig. 8 we compare the optimized photon waveform, produced at the frequency of vibration $\Omega/(2\pi) = 10.2$ MHz, to the waveform, plotted for the parameter values used in the experiment [19]. The photon waveform in the proof-of-principle experiment [19] (red dotted curve) was produced in a stainless steel film with natural abundance, 2.2%, of ^{57}Fe in iron fraction. This resulted in strong photoelectric absorption, $T_e \simeq 1.27$. As a result the peak pulse intensity was $I_{\max}(2\%)/I_0 \simeq 0.3$. The only enrichment of the stainless steel absorber by the resonant nuclei to 90% in iron fraction results in reduction of photoelectric absorption to $T_e \simeq 0.1$ and increasing the photon transmission as a whole. As a result, the peak pulse intensity also increases to $I_{\max}(90\%)/I_0 \simeq 1.04$ (green dashed curve). Although the peak pulse intensity in this case only slightly exceeds the intensity at the front of the incident photon, the enhancement in peak pulse intensity due to enrichment is about 3.5 times. However, the pulse contrast, defined as the normalized difference between intensities at maximum and the left minimum, $m = (I_{\max} - I_{\min}^{\text{left}})/(I_{\max} + I_{\min}^{\text{left}})$, is only $m(90\%) \simeq 0.35$. Optimization of the absorber's Mössbauer thickness accounting for interference of pulses with dynamical beats and the off-resonant forward-scattered

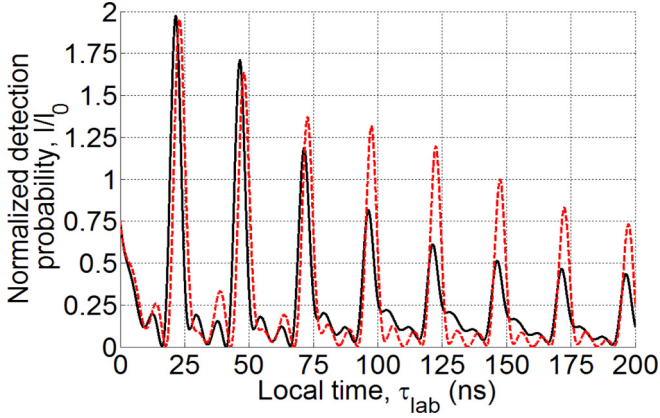


FIG. 9. Output photon waveforms in the cases of (i) suppression of the minus first sideband of the photon field via its resonant absorption (black solid line) and (ii) π phase shift of the minus first sideband via the resonant dispersion (red dashed line). The frequency of vibration is $\Omega/(2\pi) = 40$ MHz. Highest excess of the red curve over the black one is achieved for the pulse centered at $\tau_{lab} \simeq 122.6$ ns.

field (blue solid curve) results in (i) enhancement in peak pulse intensity to $I_{max}^{opt}/I_0 \simeq 1.6$ and (ii) enhancement in the pulse contrast to $m_{opt} \simeq 1$. Thus, the optimization allows producing the well-shaped high-contrast pulses with maximum detection probability of the transformed photon considerably exceeding the maximum detection probability of the photon emitted by the source.

V. γ -RAY PULSE FORMATION VIA FLIP OF THE PHASE-MISALIGNED SIDEBAND

Up to now we considered the possibilities for transforming the waveform of the incident photon into the pulse train via suppression of the antiphase (phase-misaligned) minus first sideband of the photon field by means of its resonant absorption. However, instead of suppression, this sideband can be made in-phase (phase aligned) with respect to the other sidebands of the photon field via the resonant dispersion of the absorber. In order to do this, one needs to provide π phase shift at the central frequency of the minus first sideband, which implies detuning of its central frequency from the frequency of the resonance by the value

$$\Delta\omega_{-1} = \omega_a - \omega_s + \Omega = \frac{T_M \gamma_a}{4\pi} + \gamma_a \sqrt{\left(\frac{T_M}{4\pi}\right)^2 - 1}. \quad (27)$$

Similarly to the case of absorption of the minus first sideband, studied above, we performed a numerical search for the optimal conditions, maximizing the output photon detection probability (18) after transmission through the resonant absorber, which provides π phase shift of the minus first sideband of the photon field. At the frequency of vibration $\Omega/2\pi = 40$ MHz the optimal parameters are $T_M \simeq 50$, $\vartheta_0 \simeq 7\pi/6$, and $\Delta\omega_{-1}/(2\pi) \simeq 4.4$ MHz. The corresponding waveform of the output photon is shown in Fig. 9 by the red dashed line along with the optimized waveform for the

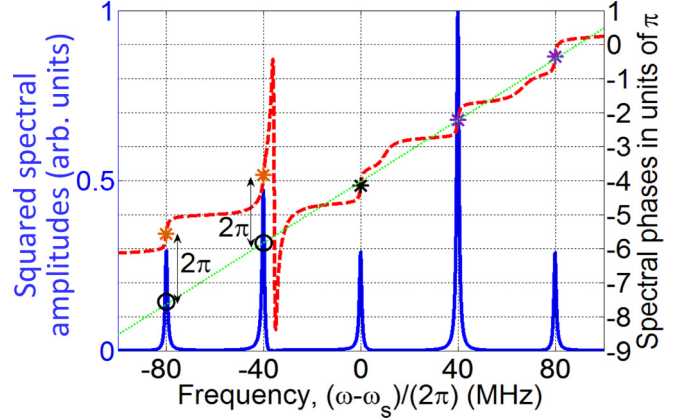


FIG. 10. The same as in Fig. 2, but after transmission of the photon through the resonant absorber. The absorber parameters $T_M = 50$, $\vartheta_0 = 7\pi/6$, and $\Delta\omega_{-1} = 4.4$ MHz are chosen in such a way that the photon field at the central frequency of the minus first sideband acquires a π phase shift. All (five) of the considerably nonzero spectral components of the output photon field are phase aligned.

case of suppression of the minus first sideband, plotted by the black solid line. The spectrum of the output photon field in the vibrating reference frame in the case of π phase shift of central frequency of the minus first sideband is shown in Fig. 10. One may expect that, since instead of deletion of the antiphase sideband of the photon field it is tuned in-phase with the others, the peak detection probability of the output photon should increase. This is true starting from the third pulse in the train and for the overall detection probability of the output photon (the detection probability within a sufficiently long time interval), as well as for the case of time averaging of detection probability over the instants of formation of the excited state of the radiating nucleus [22]. At the same time, the highest detection probability, achieved at the peak of the first pulse, is larger in the case of suppression of the minus first sideband via the resonant absorption. In order to understand this, one needs to take into account the effect of group velocity dispersion on the field of the minus first sideband. As follows from Eqs. (9), (13), and (14), the real part of the wave number of the photon field strength in the vibrating reference frame is

$$k = \frac{\omega}{c} + \frac{T_M}{2L} \frac{\gamma_a (\omega_a - \omega)}{\gamma_a^2 + (\omega_a - \omega)^2}. \quad (28)$$

This leads to the expression for the group velocity, $v_{gr} = d\omega/dk$, in the form

$$\frac{1}{v_{gr}} = \frac{1}{c} + \frac{T_M \gamma_a}{2L} \frac{(\omega_a - \omega)^2 - \gamma_a^2}{[(\omega_a - \omega)^2 + \gamma_a^2]^2}. \quad (29)$$

Since the minus first sideband of the photon field is much closer to the resonance than the others, one may take into account the effect of the group velocity dispersion only on this sideband. Thus, for the minus first sideband one has $\frac{1}{v_{gr}} = \frac{1}{c} + \frac{T_M \gamma_a}{2L} \frac{\Delta\omega_{-1}^2 - \gamma_a^2}{[\Delta\omega_{-1}^2 + \gamma_a^2]^2}$, while for the other spectral components one can assume $\frac{1}{v_{gr}} \simeq \frac{1}{c}$ (since in the considered case $\Omega \simeq 71\gamma_a$). This difference in group velocities leads to a delay of the field

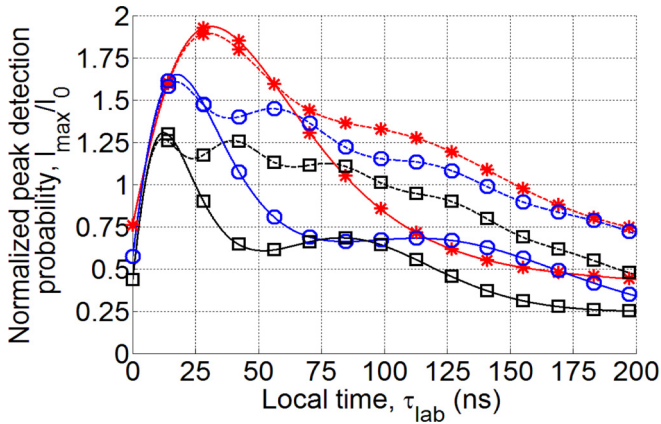


FIG. 11. Envelopes of the pulse trains, corresponding to the output photon waveforms, produced via absorption of the minus first sideband of the photon field (solid lines) and via its π phase shift (dashed lines). The frequency of the absorber's vibration is $\Omega/(2\pi) = 40$ MHz. Red color and stars correspond to the curves plotted for $T_M = 50$, blue color and circles indicate the curves plotted for $T_M = 100$, and black color and squares mark the curves corresponding to $T_M = 150$.

of the minus first sideband with respect to the others by the value $\tau_d = \frac{T_M \gamma_a}{2} \frac{\Delta\omega_{-1}^2 - \gamma_a^2}{[\Delta\omega_{-1}^2 + \gamma_a^2]}$. In the optimal case considered in Figs. 10 and 11 the delay is $\tau_d = 110$ ns, which gives a good estimate for the moment of time, at which π phase shift of the minus first sideband provides the biggest increase in the amplitude of the pulses, with respect to the case of suppression of this sideband (see Fig. 9). In a sufficiently thick absorber, $T_M \gg 4\pi$, the optimal value of detuning satisfies the relation $\Delta\omega_{-1} \simeq T_M \gamma_a / 2\pi$, so that the group delay of the minus first sideband is $\tau_d \simeq 2\pi^2 / (T_M \gamma_a)$. Thus, the delay of the minus first sideband decreases with increasing absorber thickness, as shown in Fig. 10, where we plot the analytically calculated envelopes of the pulses, produced from the waveform of the incident photon (i) via π phase shift of the minus first sideband, Eqs. (18) and (27), and (ii) via the resonant absorption of this sideband, Eq. (21). The calculations were done for $T_M = 50, 100$, and 150 , and optimal values of the other parameters. For all the considered values of Mössbauer thickness, the highest detection probability is achieved in the case of suppression of the minus first sideband via the resonant absorption. However, the resonant dispersion provides an additional tool for manipulation of the photon waveform

and allows one to get higher average detection probability of the transmitted photon.

VI. CONCLUSION

In this paper we discussed the ultimate capabilities for transformation of the exponentially decaying waveform of a Mössbauer 14.4-keV photon from a ^{57}Co radioactive source into a regular sequence of the shortest pulses with the highest temporal photon detection probability in an optically deep sinusoidally vibrating ^{57}Fe recoilless resonant absorber. We showed that the shortest pulse duration that could be produced by the discussed technique is limited by the highest available vibration frequency of the piezoelectric transducer and at present can be as short as 7.7 ps. The highest temporal detection probability of the photon is determined by the optimal conditions (optical depth of the absorber, frequency, and initial phase of its vibration) providing simultaneously (i) the largest amplitude of both incident and resonant coherently forward-scattered fields of the single-photon wave packet and (ii) the constructive interference of these fields. In the case of stainless steel absorber with 90% enrichment by ^{57}Fe nuclide in iron fraction, the highest achievable peak detection probability of the photon at the exit from the absorber is about two times higher than the peak detection probability of the photon emitted by the source. It is achieved under experimentally feasible conditions with a stainless steel film of $\simeq 4.4$ - μm physical length, vibrating with $\simeq 30$ -MHz frequency.

Manipulating a single-photon waveform can be used for quantum information processing as well as for the development of a table-top single-photon source of hard-x-ray- γ -ray pulses for the Mössbauer spectroscopy of various nonstationary processes with time resolution up to 10 ps.

ACKNOWLEDGMENTS

We acknowledge support by Russian Foundation for Basic Research (RFBR, Grants No. 16-32-60173, No. 16-02-01034, and No. 18-32-00774), as well as support by National Science Foundation (NSF, Grant No. PHY-150-64-67). The numerical studies presented in Secs. III–V were supported by the Ministry of Science and Higher Education of the Russian Federation under Contract No. 14.W03.31.0032. V.A.A. acknowledges support by the Foundation for the Advancement of Theoretical Physics and Mathematics “BASIS”. Y.V.R. acknowledges financial support (analytical studies in Secs. III–IV) from the Government of the Russian Federation (Mega-Grant No. 14.W03.31.0028).

- [1] F. Vagizov, The splitting of hyperfine lines in ^{57}Fe nuclei in RF magnetic field, *Hyper. Interact.* **61**, 1359 (1990).
- [2] P. Helistö, I. Tittonen, M. Lippmaa, and T. Katila, Gamma Echo, *Phys. Rev. Lett.* **66**, 2037 (1991).
- [3] Yu. V. Shvyd'ko, T. Hertrich, U. van Bürck, E. Gerdau, O. Leupold, J. Metge, H. D. Rüter, S. Schwendy, G. V. Smirnov, W. Potzel, and P. Schindelmann, Storage of Nuclear Excitation Energy through Magnetic Switching, *Phys. Rev. Lett.* **77**, 3232 (1996).

- [4] R. Coussement, Y. Rostovtsev, J. Odeurs, G. Neyens, H. Muramatsu, S. Gheysen, R. Callens, K. Vyvey, G. Kozyreff, P. Mandel, R. Shakhmuratov, and O. Kocharovskaya, Controlling Absorption of Gamma Radiation via Nuclear Level Anticrossing, *Phys. Rev. Lett.* **89**, 107601 (2002).
- [5] R. N. Shakhmuratov, F. Vagizov, J. Odeurs, and O. Kocharovskaya, Slow γ -photon with a doublet structure: Time delay via a transition from destructive to constructive interference of collectively scattered radiation with the incoming photon, *Phys. Rev. A* **80**, 063805 (2009).

- [6] B. W. Adams, C. Buth, S. M. Cavaletto, J. Evers, Z. Harman, C. H. Keitel, A. Pálffy, A. Picón, R. Röhlsberger, Yu. Rostovtsev, and K. Tamasaku, X-ray quantum optics, *J. Mod. Opt.* **60**, 2 (2013).
- [7] S. Shwartz, R. N. Coffee, J. M. Feldkamp, Y. Feng, J. B. Hastings, G. Y. Ying, and S. E. Harris, X-Ray Parametric Down-Conversion in the Langevin Regime, *Phys. Rev. Lett.* **109**, 013602 (2012).
- [8] R. Röhlsberger, H.-C. Wille, K. Schlage, and B. Sahoo, Electromagnetically induced transparency with resonant nuclei in a cavity, *Nature* **482**, 199 (2012).
- [9] R. Röhlsberger, K. Schlage, B. Sahoo, S. Couet, and R. Ruffer, Collective Lamb shift in single-photon superradiance, *Science* **328**, 1248 (2010).
- [10] K. P. Heeg, H.-C. Wille, K. Schlage, T. Guryeva, D. Schumacher, I. Uschmann, K. S. Schulze, B. Marx, T. Kämpfer, G. G. Paulus, R. Röhlsberger, and J. Evers, Vacuum-Assisted Generation and Control of Atomic Coherences at X-Ray Energies, *Phys. Rev. Lett.* **111**, 073601 (2013).
- [11] R. Shakhmuratov, F. Vagizov, and O. Kocharovskaya, Single γ -photon revival and radiation burst in a sandwich absorber, *Phys. Rev. A* **87**, 013807 (2013).
- [12] K. P. Heeg, C. Ott, D. Schumacher, H.-C. Wille, R. Röhlsberger, T. Pfeifer, and J. Evers, Interferometric Phase Detection at X-Ray Energies via Fano Resonance Control, *Phys. Rev. Lett.* **114**, 207401 (2015).
- [13] K. P. Heeg, J. Haber, D. Schumacher, L. Bocklage, H.-C. Wille, K. S. Schulze, R. Loetzsch, I. Uschmann, G. G. Paulus, R. Ruffer, R. Röhlsberger, and J. Evers, Tunable Subluminal Propagation of Narrow-band X-Ray Pulses, *Phys. Rev. Lett.* **114**, 203601 (2015).
- [14] K. P. Heeg, A. Kaldun, C. Strohm, P. Reiser, C. Ott, R. Subramanian, D. Lentrodt, J. Haber, H.-C. Wille, S. Goerttler, R. Ruffer, C. H. Keitel, R. Röhlsberger, T. Pfeifer, and J. Evers, Spectral narrowing of x-ray pulses for precision spectroscopy with nuclear resonances, *Science* **357**, 375 (2017).
- [15] J. Haber, X. Kong, C. Strohm, S. Willing, J. Gollwitzer, L. Bocklage, R. Ruffer, A. Pálffy, and R. Röhlsberger, Rabi oscillations of x-ray radiation between two nuclear ensembles, *Nat. Photon.*, **11**, 720 (2017).
- [16] J. Gunst, C. H. Keitel, and A. Pálffy, Logical operations with single x-ray photons via dynamically-controlled nuclear resonances, *Sci. Rep.* **6**, 25136 (2016).
- [17] W.-T. Liao, C. H. Keitel, and A. Pálffy, X-ray-generated heralded macroscopical quantum entanglement of two nuclear ensembles, *Sci. Rep.* **6**, 33361 (2016).
- [18] X. Kong and A. Pálffy, Stopping Narrow-Band X-Ray Pulses in Nuclear Media, *Phys. Rev. Lett.* **116**, 197402 (2016).
- [19] F. Vagizov, V. Antonov, Y. V. Radeonychev, R. N. Shakhmuratov, and O. Kocharovskaya, Coherent control of the waveforms of recoilless γ -photons, *Nature* **508**, 80 (2014).
- [20] R. N. Shakhmuratov, F. G. Vagizov, V. A. Antonov, Y. V. Radeonychev, M. O. Scully, and O. Kocharovskaya, Transformation of a single-photon field into bunches of pulses, *Phys. Rev. A* **92**, 023836 (2015).
- [21] Y. V. Radeonychev, V. A. Antonov, F. G. Vagizov, R. N. Shakhmuratov, and O. Kocharovskaya, Conversion of recoilless γ -radiation into a periodic sequence of short intense pulses in a set of several sequentially placed resonant absorbers, *Phys. Rev. A* **92**, 043808 (2015).
- [22] V. A. Antonov, Y. V. Radeonychev, and O. Kocharovskaya, γ -ray-pulse formation in a vibrating recoilless resonant absorber, *Phys. Rev. A* **92**, 023841 (2015).
- [23] F. J. Lynch, R. E. Holland, and M. Hamermesh, Time dependence of resonantly filtered gamma rays from Fe^{57} , *Phys. Rev.* **120**, 513 (1960).
- [24] S. M. Harris, Quantum mechanical calculation of Mössbauer transmission, *Phys. Rev.* **124**, 1178 (1961).
- [25] E. Ikonen, P. Helistö, T. Katila, and K. Riski, Coherent transient effects due to phase modulation of recoilless γ radiation, *Phys. Rev. A* **32**, 2298 (1985).
- [26] G. V. Smirnov, General properties of nuclear resonant scattering, *Hyper. Interact.*, **123/124**, 31 (1999).
- [27] Yu. V. Shvyd'ko and G. V. Smirnov, Enhanced yield into the radiative channel in Raman nuclear resonant forward scattering, *J. Phys.: Condens. Matter* **4**, 2663 (1992).
- [28] L. T. Tsankov, The spectrum of Mössbauer radiation passed through a vibrating resonant medium, *J. Phys. A: Math. Gen.* **13**, 2959 (1980).
- [29] M. D. Crisp, Propagation of small-area pulses of coherent light through a resonant medium, *Phys. Rev. A* **1**, 1604 (1970).
- [30] M. J. Berger, J. H. Hubbell, S. M. Seltzer, J. Chang, J. S. Coursey, R. Sukumar, D. S. Zucker, and K. Olsen, *XCOM Photon Cross Sections Database (version 1.5)* (National Institute of Standards and Technology, Gaithersburg, MD, 2010), Online Available: <http://physics.nist.gov/xcom>.
- [31] B. P. Sorokin, G. M. Kvashnin, A. P. Volkov, V. S. Bormashov, V. V. Aksenonov, M. S. Kuznetsov, G. I. Gordeev, and A. V. Telichko, AlN/single crystalline diamond piezoelectric structure as a high overtone bulk acoustic resonator, *Appl. Phys. Lett.* **102**, 113507 (2013).
- [32] A. Ambrosy and K. Holdik, Piezoelectric PVDF films as ultrasonic transducers, *J. Phys. E: Sci. Instrum.* **17**, 856 (1984).